# EFFECTS OF SHAPE AND SIZE OF GOLD NANOPARTICLES ON THE PROPERTIES OF COLLOID AND NANOCOMPOSITE

A Thesis

by

TAHIRA ZARRIN

Submitted to the Office of Graduate Studies of
Texas A&M University
in partial fulfillment of the requirements for the degree of

MASTER OF SCIENCE

May 2009

Major Subject: Mechanical Engineering

# EFFECTS OF SHAPE AND SIZE OF GOLD NANOPARTICLES

# ON THE PROPERTIES OF COLLOID AND NANOCOMPOSITE

A Thesis

by

TAHIRA ZARRIN

Submitted to the Office of Graduate Studies of
Texas A&M University
in partial fulfillment of the requirements for the degree of

MASTER OF SCIENCE

Approved by:

Chair of Committee, Hong Liang
Committee Members, Xin Lin Gao
Miladin Radovic
Head of Department, Dennis O'Neal

May 2009

Major Subject: Mechanical Engineering

# ABSTRACT

Effects of Shape and Size of Gold Nanoparticles

on the Properties of Colloid and Nanocomposite.

(May 2009)

Tahira Zarrin, B.E., NED University of Engineering & Technology, Karachi, Pakistan

Chair of Advisory Committee: Dr. Hong Liang

For more than a decade nanomaterials have attained huge attraction owing to the exceptionally different and excellent characteristics as compared to their bulk form. In the present research, we focus on understanding the properties and performance of nanocomposites in solid and liquid states. There are three major areas involved in this thesis research. Firstly, we will identify effective methods or techniques to evaluate nanomaterials. Conventional and non-conventional techniques will be implied. The second part is to study the interfacial reactions between nanoparticles (NPs) and fluid molecules. This is to obtain basic understanding of nanoparticles and their interactions with matrix materials. Thirdly, we will investigate the mechanical properties of nanocomposites.

Experimental results showed that the mechanical properties of nanocomposites measured at macroscale exhibited differences when the shape and size of gold NPs were changed. The morphological characteristics of the material were shown effectively at the nanoscale based on the NPs' shape and size. The properties of NPs influenced the

properties of gold colloid. Such changes were the result of the interfacial interaction of gold NPs and the host material.

# DEDICATION

*To my dearest*

*Ammi & Abbou*

# ACKNOWLEDGEMENTS

Alhumdulillah (All praise belongs to Allah)

I greatly appreciate my committee chair Dr. Liang for her constant support and encouragement during this research. Without her kindness and patience, this thesis would not have been completed or written. I have sincere gratitude for the members of my thesis committee, Dr. Gao and Dr. Radovic and for their sincere contributions. I also appreciate Dr. Radovic for permitting me to use his lab and his students Windy, Patrick, and Ramon for help during the experimental stage. Also, I would like to mention my friendly, cheerful and helpful colleagues of the surface science lab, especially Dr. Subrata Kundu, for synthesis of nanoparticles and Lee, Ke and David for helping me test the samples for my research. I give my special thanks to Dr. S. C. Lau and Dr. Angie Hill Price (ETID Department) for their kind consideration of students, and especially for helping new international students.

Thanks to my friends in College Station; without them I might not have enjoyed these two years at Texas A&M University. Finally, I dedicate special thanks to my honorable, precious and most deserving parents and siblings for their love, support and encouragement.

This research was partially supported by the National Science Foundation (grant numbers 0506082 and 0535578), Texas Engineering Experiment Station (TEES), and the Department of Mechanical Engineering, Texas A&M University.

# NOMENCLATURE

| | |
|---|---|
| Au | Aurum |
| NPs | Nanoparticles |

# TABLE OF CONTENTS

Page

# LIST OF FIGURES

Page

Page

# LIST OF TABLES

# CHAPTER I

# INTRODUCTION

This chapter provides a brief introduction of the factors that influence the mechanical properties of metallic materials at macro and nanoscales. Some of the most common techniques that are used to determine the mechanical properties of metallic nanoparticles are discussed briefly. The main intention here is to build up a correlation of structure-properties materials at different scales.

## **1.1.** Introduction

The word ‘Nano’ came from Greek word ‘dwarf’ [1,2,3] which means ‘very small’. In metric system it refers to one billionth [1,2,3,4] and the nanometer [1,2,3,4] is thus one billionth of a meter. Nanoparticles (NPs) generally refer to particles with sizes less than 100 nm[1,2,3,4]. Nanoparticles are zero dimensional nanostructure with at least one dimension less than 100nm [1,2,3,4]. NPs can be synthesized mechanically[5,6] and chemically[7,8,9,10] into different shapes and sizes. When the NPs are suspended in solid, liquid, or gas they are called colloidal [1,2,3]. Colloidal is the mixture of two different phases: an incessant phase like a gas or liquid and a solid discrete phase e.g. partcles. The dispersed phase (NPs) size can be between 5 to 200nm [1,2,3]. Since the particle size is in nanometer range these NPs are invisible to the naked eye. These colloidals are sometimes also referred to as colloidal solution or colloidal suspension[1, 2].

---

This thesis follows the style of Applied Physics Letters.

Due to the size effect, the properties of nanoparticles greatly differ from their bulk. The metallic nanoparticles generally show unique mechanical [11,12,13] physical [14,15,16], electrical [17,18,19], optical [20,21,22], magnetic [23,24], and morphological/structural properties [25,26,27]. With reducing size, the materials properties are seen to be enhanced [28,29]. There is a wide number of applications of nanomaterials. [29,30,31]. Nano-structured materials including thin films have several applications such as reinforcement material for structural purposes[32,33], as protective coatings for magnetic hard disks[34], as nanocomposites such as nano-structured low carbon steel with high tensile strength,[30] and as additives in abrasion resistant coatings[35]. Nanomaterials of low weight, high strength with high electrical resistance have applications in micro- and nano-electromechanical systems[36,37]. Among all mentioned applications, mechanical properties play important roles.

In order to better understand the topics discussed in this thesis, factors affecting the mechanical properties of nanomaterials will be described. The main focus of this chapter is to develop an idea as to why the mechanical properties of metallic materials at macro scale and at nanoscale exhibit differences. In addition, this chapter discusses the important roles of these factors and the experimental techniques used to measure the mechanical properties of metallic nanoparticles.

## **1.2.** Factors Affecting the Mechanical Properties of Metallic Material at Macroscale

### **1.2.1.** Bonding Types and Structures

Bonding types and lattice structures are main factors affecting the mechanical properties of materials[2,29,38]. Both elastic[2,29,38]-and plastic[2,29,38] properties of materials are influenced by the bonding types and lattice structures. Within the elastic range, the ratio of the axially applied stress to the resultant strain ~~is~~ defined as Young's Modulus [1,2]. The elastic modulus depends on how easily adjacent atoms can be stretched under an applied load and can recover when unloaded[1,2]. This is directly related to the bonding type. The higher the bond energy the more difficult it is to stretch the atoms[1,2,39].

The strain in the material under uniaxial tension or compression is related to the bonding type and lattice structure. Metallic bonds are highly unidirectional and have densely packed structures [1,2,39]. Figure 1.1 shows how the positive cations are surrounded by electron clouds in a metal to form metallic bonds.

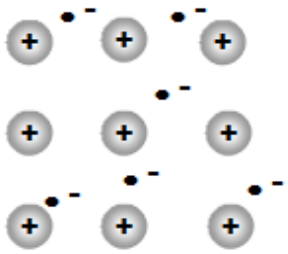

FIG. 1.1. Illustration of metallic bonding (positive cat-ions and electron cloud) [39]

Due to the nature of metallic bonding in metallic materials, the deformation is relatively easy as compare to the covalent and ionic bonding [39]. The lattice structures of metallic materials have slip planes which help in plastic deformation in metals [39]. Figure 1.2 shows three different lattice structures adopted by different metallic materials.

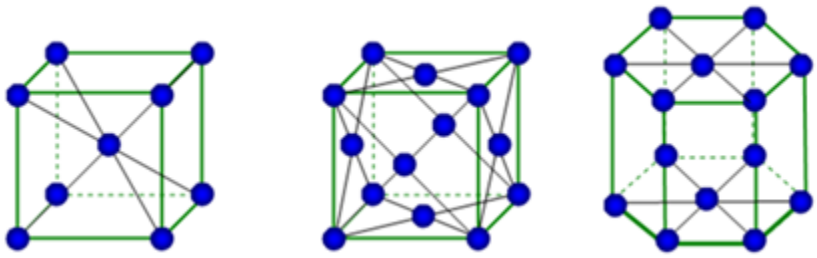

| Cubic Body Centered | Cubic Face Centered | Hexagonal Closed Pack |
|---|---|---|
| **Fe, V, Cr** | **Al, Cu, Au** | **Zn, Mg, Cd** |

FIG. 1.2. Crystal lattice examples[39]

### **1.2.2.** Defects in Crystal Structure

The arrangement of atoms in a bulk material is not in perfect order and generally has lots of imperfections (point, line and planar defects) [1,2,39]. The line defects in crystal lattice which are called dislocations and they are the primary source [39,40] of plastic deformation in the material under an applied load. Figure 1.3 shows one of these imperfections called edge dislocation. Dislocations help in the sequential movement of atoms in the material, resulting in deformation. The stress field around a grain boundary restricts the movement of dislocation [39,40].

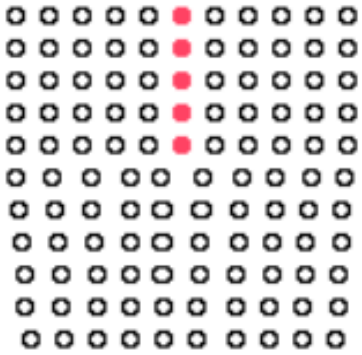

FIG. 1.3. Example of dislocation (edge) caused by an extra half plane of atoms[39]

### **1.2.3.** Grain Size and Grain Boundaries

Grain size [39,40] has substantial effects on the mechanical properties of polycrystals. Grain size refinement can increase the strength and hardness [39,40] of the material and reduce ductility [39,40]. The reason is that during deformation these refined grains offer resistance to dislocation motion. During deformation, the number of grains increases greatly and so do the grain boundaries. Grain boundaries offer resistance to the motion of dislocations [39, 40]. The reason behind this resistance is the generation of stress fields around the grain boundaries. That is why the strength of materials can be changed by modifying the size of grains and the number of grains per unit area–[41, 42]. This behavior was described through the Hall-Petch relation [1, 2].

Creep, which is the slow deformation in material under a constant stress, [39, 40] is also affected by the grain size. The grain size reduction in materials not only adds to the grains but also to the number of grain boundaries. In addition, the ultrafine grain size amplifies the number of atoms at the border of grains. When a shear stress is applied to

such materials the grains can slide and cause a poor resistance to creep. Improvement in creep is caused by the enhanced diffusion between the atoms of adjacent grains. Conversely, a coarse grain is expected to offer more resistance to creep [1, 2]. Ductility is another important property of materials, which is the measure of plastic deformation in the material without fracture[1, 2]. Like other plastic properties of materials, ductility is also affected by the grain size.

In the next section we will describe the factors that-affect the mechanical properties of metallic nanoparticles.

## **1.3.** Factors Affecting the Mechanical Properties of Metallic Material at Nanoscale

### **1.3.1.** Bonding Types and Crystal Structures

It has been reported that the gold nanoparticles have highly symmetric cubical, octahedral, and rhomb-dodecahedral structures when the particle size is above Ø10 nm [1, 2, 43, 44]. For particle size less than Ø 10 nm, it was reported that icosahedrons and decahedrons dominate the crystal structure [43-46]. The presence of different crystal structures at different nanoscales is directly related to high surface energy. Decreasing the particle size in nm range sharply increases the number of surface atoms. The unsaturated surface atoms cause energy imbalance in the particle. Also these surface atoms squeeze the inner atoms, causing complex strain in the particles. This energy imbalance forces the particles to adopt the structure that can minimize its energy. The presence of different crystal structures at nanoscale is therefore related to the minimization of energy due to the size reduction. The packing density and the surface

energy dominate the behavior of materials at the small length scale while the strain energy affects a material at a comparatively large length scale. It was reported by Cleveland [47] and Pail[48] that in case of gold, the energy minimizing mechanism mostly tended to adopt faceted shapes. During faceting, the nanoparticles minimized the strain energy in the atoms and the surface energy of the particle. In the presence of organic molecules, gold nanoparticles tended to adopt more faceted shape structures to minimize the energy [49]. From the literature review, it seems that several mechanisms of minimizing[50] energy control the formation of microstructures at the nanoscale.

### **1.3.2.** Ultrafine Grains and Grain Boundaries

Generally–equiaxed grains exist in nanophase materials. –Nanophase materials can -deviate from this structure for efficient packing (nanophase material can have many local minima) [2, 50]. Due to the fine grain size a good proportion of atoms occupy grain boundaries. It was reported that for spherical particles of 5 to 10 nm average grain diameter, the atoms at the grain boundaries ranged from 15 to 50% [29] thus the grain boundaries affected the mechanical properties of nanomaterials. Research of nanomaterials using XRD[51], EXAFS[52], Mossbauer spectroscopy[53,54] has revealed that the orientation of grain boundaries was quite random as compared to the bulk where the grain boundaries might be in either short or long range order[1,29]. Conflicting results have been reported regarding the dependence of elastic modulus of nanomaterials on the grain size[55]. Some results suggested that elastic modulus decreased with the reduction in grain size[56] and some results suggested that elastic modulus was independent of the grain size

[57]. Some authors reported that in case of crystalline gold, the reduction in grain size actually increased the value of elastic modulus [58]. Many authors reported that other elastic constants like shear modulus was dependent on the interface distance and also that elastic modulus increased with decreased spacing between atoms[59, 60]. Some other mechanical properties like creep that mostly occur due to diffusion, became more active at the small scale due to the short distance between grains and the large portion of atoms in grain boundaries.

### **1.3.3.** Dislocations

It was reported that dislocations are rarely present in nanomaterials [61-64]. Due to the movement of these dislocations, permanent deformation occurred in bulk material. In the case of nanomaterials, their presence was limited in the grain [65, 66] and mostly they couldn't move in the grain or were frozen. If new mobile dislocations were created, the plastic flow would be possible. An example was given by Siegel [29] for the mobility of Frank Reed dislocation in the grains of a nanomaterial. The Frank Reed dislocation was pinned at both ends and when the force was applied, the dislocation could bow out. In those types of dislocations, the vertical movement along the slip plane was restricted due to the pinned ends. Stress needed for the movement of this dislocation was proportional to the distance between the pinned ends. Thus in the case of very small grains the movement would become difficult and the strength of material would tend to increase.

### **1.3.4.** Strain

As discussed earlier in this chapter, increased number of grain boundaries in nanoparticles induced strain[29,38]. Pores and ultrafine grains contributed to the grain boundary sliding[1,29,38]. The number of interfaces and the diffusion in between the same also add to the strain. Early theories of nanoparticles presented the idea of bulk material-like properties in the middle of the particles[68,69]. Later tests with the high energy synchrotron X-ray and analysis, using pair distribution function, revealed that outer atomic layer of nanoparticles along with the interior was strained[67]. The lattice structure was found to be similar to bulk material but was not the same[67]. The properties of nanoparticle were not the same to the bulk. This claim was in agreement with the discussion in section 1.2.2.2 that when the atoms at the outer layer of a nanoparticle surface relaxed they pushed the interior atoms inside. This created a complex strain in the inner of particle as well. As a result, the nanoparticles were not uniformly faceted[67-71].

### **1.3.5.** Porosity

It is has been reported that almost all materials at nanoscale form aggregates[1,2,29], which therefore posses porosity due to the grain boundary junction. This can also result from the deformation of the nanophase material which is always present[1,2,29]. Also it is stated that the size of these pores is in the range of the grain size of materials [29]. Atomic diffusion is also much higher due to the size effect, which also helps in plastic deformation, as compare to material at macroscopic scale having coarse grains. Porosity

presence in nanophase material is usually reported to be measured through a number of different techniques: PAS, PD, SANS & PS [71, 72, 73, 74, 75, 76,77].

Nanoscience and technology, like any other field, is facing many challenges. One of those is to formulate new materials with unique mechanical properties. As discussed earlier, at the nanoscale many of the mechanical properties of materials have changed, such as hardness, elastic modulus, toughness, and strength. It was observed that it would be difficult to identify factors that affect the mechanical properties of different metallic materials at nanoscale. As a matter of fact, if one of these factors is dominating the others, the change in properties would be different (e.g., at a scale of 5-10 nm diameter size of NPs, the porosity would be huge as compared to the particle size of slightly larger (50 to 100 nm) such that the elastic and plastic properties would be different). The factors that influence the mechanical properties at different scale are summarized in Figure 1.4. The summary indicates that superior mechanical properties are expected at nanoscale. But there are some unexpected results, such as unchanged elastic moduli of spherical gold nanoparticles down to the size of 1nm[57] while the 20% reduction in the elastic modulus of gold nanorods[57]. The challenge is to interpret these unexpected results and also to find novel methods for the investigation of mechanical properties at such a small scale.

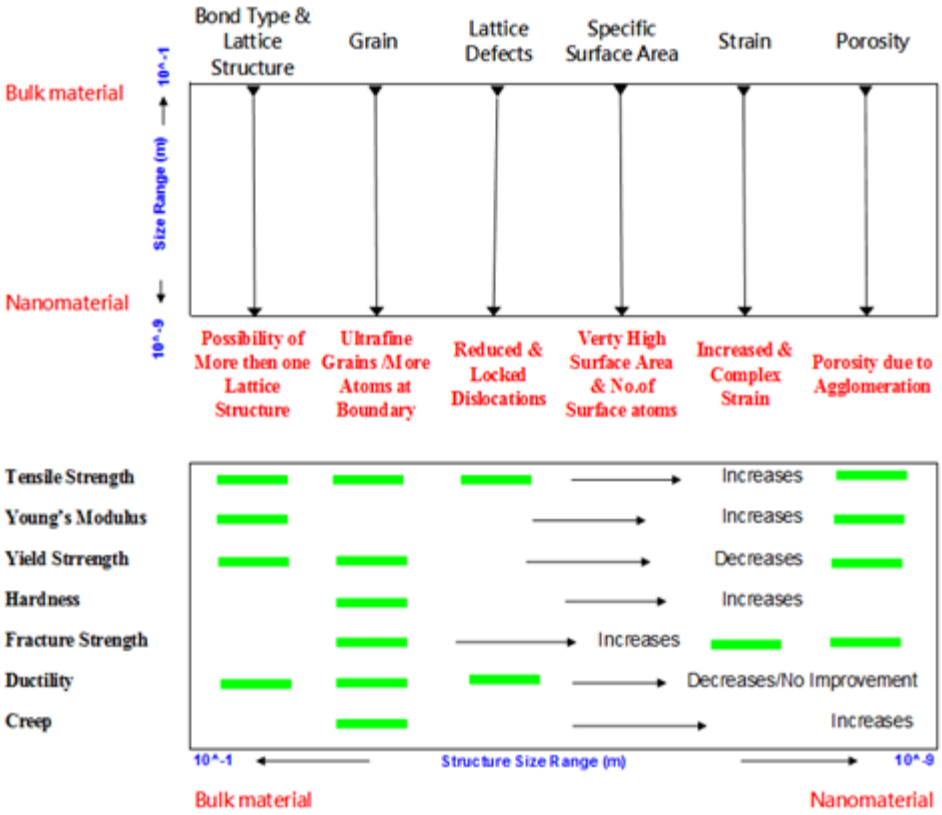


FIG. 1.4. Factors affecting the mechanical properties of metallic materials at different scales

Until now, the emphasis has been on the effects of size on materials properties. The next section will provide a review on different experimental techniques, generally considered to determine the elastic properties of metallic materials at nanoscale.

## 1.4. Experimental Evaluation of Mechanical Properties of Metallic Materials at Nanoscale-Techniques

### 1.4.1. Atomic Force Microscopy (AFM) Applications and Limitations (Nano-Mechanical Measurements)

***Principle***

In an Atomic Force Microscope (AFM) a nanometer sized sharp probe is attached to a micro-machined cantilever beam. With the application of a small force the tip of the probe touches the material surface. The deflection of the tip is kept constant, but the distance which is adjusted to keep this deflection constant due to the irregularities in the surface is recorded. Figure 1.5 shows the schematic of AFM. In the noncontact mode, the deflection is not kept constant and is recorded as the tip of the probe approach the vicinity of material surface. The response of the tip of probe is recorded. That response is related to the stiffness of the material. In this way a complete force deflection curve can be obtained which can give the elastic properties of the material[1,2, 3,4]. This method was successfully used to determine the elastic modulus, through calculation, of a single atom[78].

***Applications and Limitations (Nano-Mechanical Measurements)***

**Force Distance Curve**

The AFM probe above the sample surface is pressed with a force F (typically in nN range) against the surface. The repulsion of the probe in this region back into free space is recorded as the distance and the force/distance (F/D) curves will be obtained[1,2,3,4].

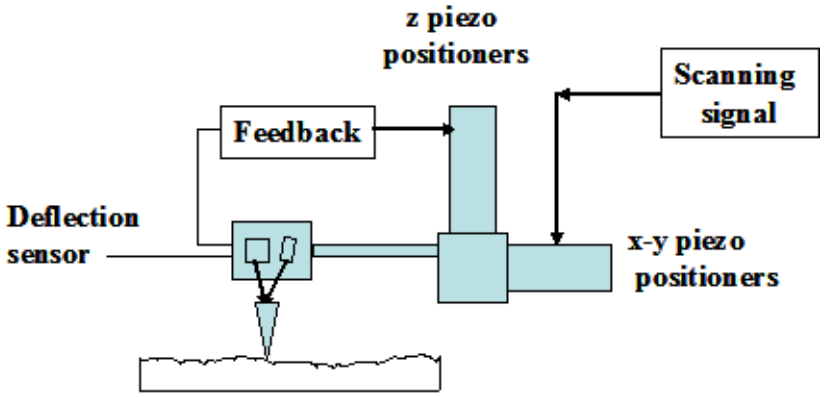


FIG. 1.5. Schematic of AFM

**Nanoindentation**

Some AFMs have nanoindentation configuration. Indentation requires that the cantilever be stiff enough as compared to the sample material. The probe also needs to be hard enough for making a nano-indent[1,2,3,4].

**Friction Coefficient**

AFM has the ability to measure both vertical and horizontal forces. With this capability, an AFM can provide the surface friction data at the nanoscale[1,2,3,4].

**Topographic Imaging**

AFM is a powerful imaging tool and can provide 2D and 3D topographical images of surfaces. It provides a good image resolution that can be compared with the resolution of TEM. In AFM topography can be measured through two different modes: contact mode and dynamic mode. If the tip touches the surface during scanning, the mode is called a contact mode. During this mode the cantilever movement is controlled

by the piezoelectric scanner in the z direction while the tip scans along x-axis. The profile of the surface is a plot of x vs. Δz (deflection of cantilever).

### **1.4.2.** Pump Probe Spectroscopy

***Principle***

This technique works only for metals[57]. It gives the accurate measurement of elastic properties of metal nanoparticles through the coherent excitation of conduction band electrons. This technique uses ultra fast low intensity laser pulses to excite surface electrons. The excitation energy causes the particles to expand. This expansion depends on the coefficient of thermal expansion, and the lattice temperature increase. Figure 1.6 shows how the particle starts vibrating after the laser heating (blue to pink). Coherent vibrational motion causes oscillation in the particle (pink circles).

The vibrational modes of nanoparticles can be determined by detecting the Plasmon Resonances. Time resolved spectroscopy is then used to determine the vibrational modes of material. These vibrational modes are correlated to the elastic properties of the material. The period of the mode for nanorods, is related with the aspect ratio and the properties of material, using the relation mentioned below[57].

$$T_{ex} = \frac{2L}{\sqrt{E/\rho}}$$

here *'L'* is the-nanorod length, *'ρ'* is the density, and *'E'* is the Young's Modulus of the material.

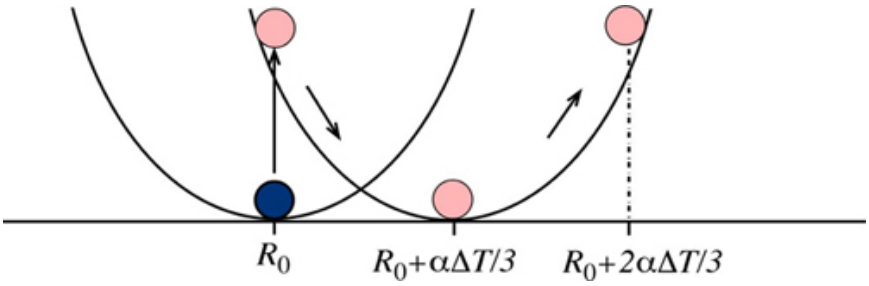


FIG. 1.6. Schematic of pump probe spectroscopy[57]

**Applications**

This experimental technique can provide the elastic modulus of metallic nanoparticles while suspended in a liquid. It does not involve any substrate interaction or any physical attachment with any solid. The results obtained are considered accurate.

**Limitations**

Though the values of elastic modulus using this method are considered accurate, the effect of laser heating on the structure of nanoparticles cannot be neglected. The data obtained using this technique needs to be investigated for any structural changes, related to nanoparticle and laser interaction. This technique can only work when particles are suspended in liquid and it works only for metallic nanoparticles.

### **1.3.3.** Rheometer

#### Principle

Rheometer is used to measure the rheology of fluids. Since a Rheometer measures the behavior of fluid under applied stress, they can be broadly classified in two types:

Shear Rheometer: measure the fluid properties under shear stress &

Extensional Rheometer: measures the fluid properties under tensile stress.

Figure 1.7 shows the schematic of the Rheometer. In this setup, the fluid is held between two parallel plates. The upper plate moves at an angular velocity and the bottom plate is fixed. During testing, a dynamic shear strain is applied to the sample and the transducer measures the resultant torque. The other properties can then be calculated using the torque data obtained during testing[79].

#### Application

The Rheometer is used to measure different properties of a fluid, such as the yield stress, shear modulus, creep, viscosity, kinetic property, etc. For nanoparticle suspended in liquid, the Rheometer is a good instrument to evaluate the particle effects on any fluid properties.

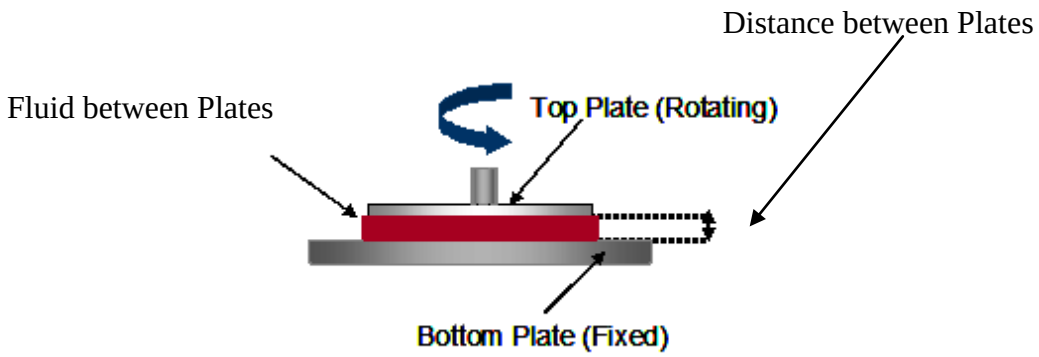


FIG. 1.7. Schematic of rheometer

Some common experimental techniques for measuring the mechanical properties of materials at different scales are summarized in Figure 1.8. This clearly shows that RUS covers a long range of measurement size, from thin films to bulk material. The principal, accuracy, and application of RUS will be discussed in the coming chapter.

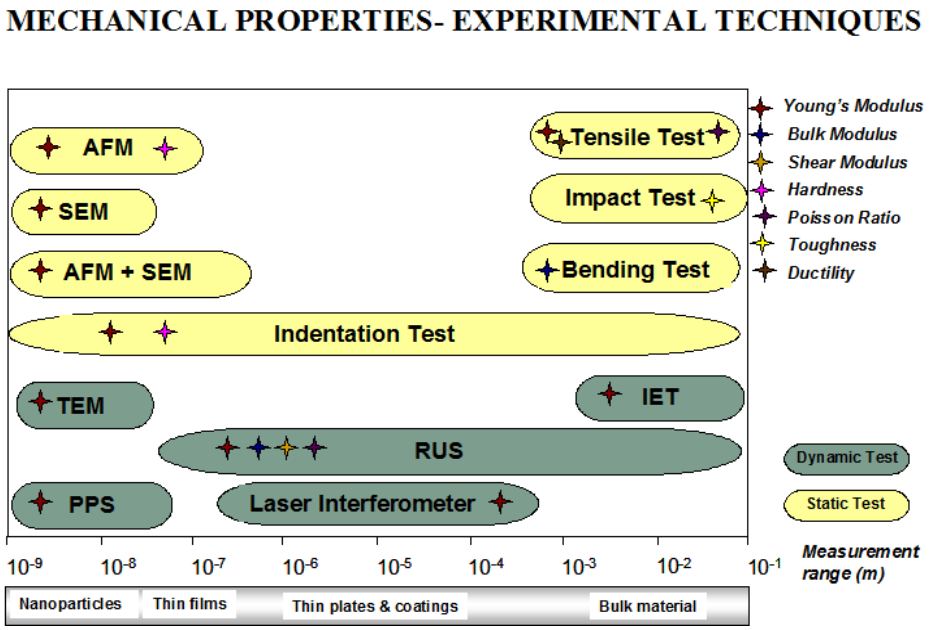


FIG. 1.8. Summary of some experimental techniques used to determine the mechanical properties of metallic materials at different scales.

List of abbreviations used in Figure 1.8.

AFM: Atomic Force Microscopy

SEM: Scanning Electron Microscope

TEM: Transmission Electron Microscope

PPS: Pump Probe Spectroscopy

RUS: Resonant Ultrasound Spectroscopy

# CHAPTER II

## MOTIVATION AND OBJECTIVE

As discussed in Chapter I, the factors that influence the mechanical properties of metals at the nanoscale need to be identified and interpreted well. Several different methods are available to evaluate these properties of metals at different scales (macro to nano) either as a particle or composite (Figure 1.8). The difficulties associated with the measurement of mechanical properties of a single nanoparticle and the limitations of available techniques have already been discussed in the previous chapter. In addition, it was mentioned that the properties of nanocomposites can be measured at a small scale using different techniques. Most of the static and dynamic techniques, as listed in Figure 1.8, are not appropriate for acquiring accurate data. Due to the limitation of instruments, precise evaluation of nanomaterial properties has yet to be achieved. The precise evaluation of mechanical properties of materials at the nanoscale is important to formulate new materials with unique properties and for novel applications.

To obtain the basic understanding of nanoparticles, this thesis has three objectives.

- Develop a methodology to characterize mechanical properties of nanoparticles and their composites.
- Investigate effects of certain factors, such as particle concentration, shape, and size on their composites in both liquid and solid states.
- Obtain fundamental understanding of nanostructure-property relationships of nanoparticles**.**

To obtain the major objectives listed above, a series of experimental approaches are proposed. A technique based on the ultrasonic excitation mechanism (Resonant Ultrasound Spectroscopy) is proposed to be used to characterize nanocomposites. The RUS is expected to be able to evaluate the complete elastic tensor of materials (metals and composites). At a micrometer length scale, we will evaluate the mechanical properties of the nanocomposite using a microscale tester and a three point bending tester.

To understand the nanostructure-properties of nanomaterials, we propose to develop a nanocomposite made of gold nanoparticles in a sorbitol matrix. The difference between gold and sorbitol is the driving force for this approach, so that the nanomaterial properties of nanoparticles are highlighted.

In order to understand the properties of nanoparticles in a liquid, rheometrical behavior will be studied. We plan to study the effects of size and shape of nanoparticles on the rheometrical properties, such as the viscosity and shear.

The research will reveal materials properties, particularly mechanical properties, of nanoparticles. The methodology developed here will be beneficial for studying other materials. The impacts of this research lie in the advancement of nanomaterials science and engineering. New understanding in structure-property relationships will be obtained.

# CHAPTER III

# MATERIALS

As discussed in the previous chapter, the properties of metallic materials differ substantially at nanoscale, and superior properties are expected at the small scale. This chapter presents the properties of gold as a bulk material and as nanoparticles and the reason of selection of gold for this experiment.

Also to test the properties of gold nanoparticle composite, sorbitol is used as a matrix material. In the later sections the properties and structure of sorbitol will be discussed in detail.

## **3.1.** Gold

### **3.1.1.** Properties of Gold at Macroscale

Gold is a noble d-block element of period 6 and group 11. The IUPAC name of gold is Aurum. It has atomic number 79 and atomic mass of 118a.m.u. Its crystal structure is face centered cubic (FCC). It is a transition metal that has an unsatisfied d-sub shell. Due to this property gold can form cat ions. Gold has five different oxidation states. As bulk the gold has good electrical and thermal properties. Gold is a very dense material also it is very malleable and can be drawn into thin sheets and wires. The stiffness of gold is also high. Gold is chemically inert for most corrosive agents, moisture, and oxygen. In ancient times, these properties of gold made it not only utilized for making coins, jewelry, and medication[80], but also very expensive. Some of the

properties of bulk gold are given in TABLE I.

TABLE I. Properties of gold at macroscale[80]

| Properties of Bulk Gold | |
|---|---|
| Structure | FCC |
| Melting Point | 1064°C |
| Thermal Conductivity | 310 W $m^{-1}$ $K^{-1}$ |
| Coef.of Thermal Expansion (25 °C) | 14.2 µm $m^{-1}$ $K^{-1}$ |
| Electrical Conductivity | 318 W $m^{-1}$ $K^{-1}$ |
| Young's Modulus | 79 GPa |
| Hardness | 25 HV |
| Speed of sound | 2030m/s |
| Resonant Frequency | 1.74 MHz |
| Density | 19.3 $g.cm^{-3}$ |
| Color | Yellow |

**3.1.2.** Why Bulk Gold?

Of all the known metals, gold is the least prone to oxidation. In addition it is a very good electron conductor. Its surface chemistry attracts sulfur containing organic molecules and is very biocompatible. Due to these properties the use of gold is nearly 5000 yrs old when it was used in Egypt especially in dentistry[81]. Founder of modern

pharmacology Paracelsus (1493-1541) developed many successful medicines from metallic minerals including gold. In nineteenth century implant of gold piece started for inflamed joints[80]. Michael Faraday also used gold to reduce dependency on alcohol, caffeine, nicotine, and carbohydrates[80, 81]. In the twentieth century gold started to be used to cauterize blood vessels. In the twenty first century bulk gold has been used along with proteins to produce important medicines[80, 81].

### **3.1.3.** Properties of Gold at Nanoscale

Only the properties and use of gold at macroscale are presented above. Now the properties of gold at nanoscale are being presented. This new section is the literature review that will cover all the properties of gold at nanoscale revealed by different researchers to date.

#### ***Heterogeneous Catalytic Ability***

This character is found in gold when its size is reduced in nanometer range and its surface energy is high. Due to this property during chemical reaction a reactant diffuses to the periphery of catalyst and after the completion of reaction diffuses out from the catalyst or desorbs from catalyst surface. This movement of reactants can control the rate of chemical reactions. To date, it is indefinite whether the property of gold at nanoscale is due to high surface area; or due to the lattice structure, that might have changed; or a result of increment in the availability of diffusion sites[82].

***Crystal Structure***

The gold maintained the same FCC structure even at nanoscale for nanosphere of Ø10 nanometers. The structure of gold nanospheres with diameter less than 10 nanometers is still not definite[2]. Four different structures were claimed for gold nanospheres of size less the 10 nanometers[57, 82]:

Truncated octahedron

Icosahedron

Decahedron

Cuboctahedron

To date, it is not clear which claim is correct.

***Melting Temperature***

The melting temperature of spherical gold nanoparticles decreases as the size of particle reduces. This decrement in melting temperature was reported for the particle size of less than 20nm. A very sharp decrement was recorded for gold nanospheres, smaller than 10 nm. The melting temperature of gold was reported to drop to 830$^{o}$C for Ø5nm sphere. Melting temperature was further declined to 200$^{o}$C for Ø1nm sphere.[83]. All experimental results have proved that this decline corresponds to the high surface energy of nanoparticles[83, 84].

***Intense Heat Emission***

In an experiment, Hug and Sasha [85] found out that when a cluster of gold nanoparticles was

### *Color*

The color of any object depends on its ability to reflect or absorb a certain wavelength of light. When the size of element becomes less than the wavelength of light, they absorb light with a specific wavelength[86]. When the nano size clusters of gold atoms hit with light energy, the free electrons of surface atoms begin to oscillate and create electron waves called surface plasmons. Then, these electron waves produce light energy which is released. The color of the light produced depends on the size and shape of the nano-cluster. A very small size nanoparticle of gold gives a ruby red color, but the cluster of gold nanoparticles can have different colors (pink or violet or blue) depending on the size of the cluster[86].

### *Electrical Properties*

#### Electron Transport Property

If the size of nanoparticle is too small, it will be quantized and no longer obeys the classical mechanics. Electrons of such particles don't need any additional energy to cross the potential barrier for minimizing the energy or to go to the lowest energy state. In such cases, electrons minimize their energy through tunneling. This happens because at nanoscale the density distribution of electrons at the surface decreases. If a gold nanoparticle is placed between two conducting electrode, without any physical contact, under an applied potential, the electrons will show the tunneling effects[87].

**Electrical Conductivity**

As the size of gold particle reduces, electrical conductivity starts decreasing. It is reported that at a particle size of 1 to 3nm, gold becomes a semiconductor with significant band gap. This band gap can be tuned to give desired electrical properties[88].

***Mechanical Properties***

**Hardness**

As the particle size decreases the hardness of the material increases[29, 89]. The reason for this is the presence of almost no defects and the ultrafine grain size which increases the strength of the material. Both Siegel's[29] and Lim & Chaudri's[89] work show that the hardness of a nanoparticle is a function of its size. Their results show that in case of gold nanospheres, the hardness increases substantially for particle size less than Ø100nm and becomes almost double of its bulk hardness, at nanoparticle size of Ø5nm.

**Young's Modulus**

It is expected that due to the small size of nanoparticles the value of elastic modulus should increase because of almost defect free structure. But it has been reported that the elastic modulus of Au nanoparticles cluster (spherical) was 2/3 of that of bulk gold[90]. In this experiment, nanoindentation and scanning probe microscopy were used. In another experiment, Gregory[57] found out that the elastic modulus of gold nanospheres (diameter 1-200nm) was the same as that of bulk. However, in case of nanorods, the elastic modulus reduced and decreased to 20% of bulk material at nanorods length of 75nm. His experiment was based on the thermal excitation of electron with laser pulses,

so the possibility of any phase change during thermal excitation may be the factor influencing this change in properties.

### **3.1.4.** Why Gold Nanoparticles?

***Tracking Device in Living Organism***

Most of the cancer cells have a layer of a protein called EFGR (Epidermal Growth Factor Receptor), which is unlikely to be present in healthy cells. The antibody of this protein is attached to gold NPs, and the same were then injected in the body. This way the particles with antibody attach to cancer cell only, making cancer detection much easy. It was also reported that Ø35 nm particle are the best to be used in this particular application. Gold is nontoxic and has a strong light absorption spectrum. Due to these two properties this application will have a promising influence on the future use of gold nanoparticles[91].

***Gold Colloidal Can Increase Mental Acuity***

Due to electron transport property, the gold colloidal was tested to increase the conductivity between nerve ends. This can help to improve the sharpness of the brain and the ability of focusing. The nerve ends have gaps between them. When a gold particle sits between nerve ends and is stimulated by an outside stimulus, it increases the conductivity between the ends and enhances the function of receptor[92].

***Gold Nanoparticles Boost Electronic Memory***

Multiple layers of gold nanoparticles were used to boost the storage density of flash memory. Flash memories used in USB sticks and memory cards for digital

cameras, normally hold a single layer of electric charge trapping device. Here gold nanoparticles were deposited in alternating layers with an insulating polymer onto a base of hafnium oxide coated silicon substrate. This led to an increase in the memory density of approximately 3.5 times in comparison to the single layered devices[93].

**3.2.** Synthesis of Negatively Charged Citrate Stabilized Gold Nanoparticles

In the present research, negatively charged Au nanoparticles (Au-NPs) were synthesized. The following lists the chemicals used for the synthesis:

Hydrogen Tetrachloro Aurate Tri-Hydrate ($HAuCl_4$, $3H_2O$, 99.9%)

Tri-Sodium Citrate Dihydrate ($Na_3C_6H_5O_7$. $2H_2O$)

Ultrapure Distilled (UPD) Water

All materials were procured from Sigma-Aldrich.

Synthesisation method used here is called Turkevich Method[94]. 1.25mL of $10^{-2}$ M aqueous gold chloride ($HAuCl_4$, $2H_2O$) solution was mixed with 48.35mL of de-ionized water. The stirring and heating of mixture was done up to 80 ºC. After heating and stirring, 0.40mL 1% tri-sodium citrate was added. After further heating for 10 to 15 minutes the wine red color of solution appeared. DI water was mixed to adjust the volume to 50mL. For concentrated gold colloid the final volume was around 20mL. In this process, sodium citrate acted as a reducing agent and reduced the $Au^3$ ions to $Au^0$. After formation, gold NPs adsorb the negatively-charged citrate ions onto the surface and helped to avoid unwanted aggregation of NPs.

We examined the average diameters of the particles using a Transmission Electron Microscope (TEM), Figure 3.1.

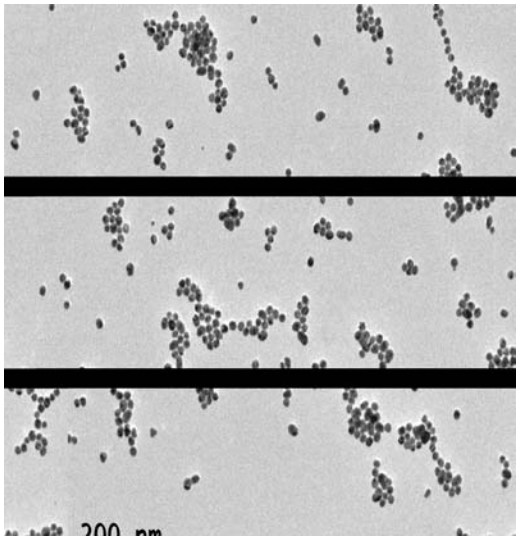


FIG. 3.1. TEM image of the citrate capped gold nanospheres (Ø20-30nm)

The different sizes of gold colloids will be used in this experiment are given in TABLE II.

TABLE II. Different Au colloid used in this research

| Particle Size ⟶ | Au-Nanospheres | | | | Au-Nanorods | |
|---|---|---|---|---|---|---|
| | Ø 8nm | Ø 20nm | Ø 55nm | Ø 75nm | Ø40nm, L=300nm | Ø=10nm, L=120nm |
| Concentration 1 (Number of NPs/ 100µL) | 4.76 x $10^{12}$ | 1.56 x $10^{11}$ | 1.47 x $10^{10}$ | 5.78 x $10^{9}$ | 8.73 x$10^{9}$ | 3.49 x $10^{10}$ |
| Concentration 2 (Number of NPs/ 100µL) | 9.52 x $10^{12}$ | 3.12 x $10^{11}$ | ----- | ----- | ------ | ------ |

All the nanospheres have the same volume of gold in the colloid. Both the nanorods colloid also has the same volume of gold.

**3.3.** Sorbitol

Sorbitol is a type of sugar alcohol. All sugar alcohols ($H(HCHO)_{n+1}H$ ) are obtained from glucose ($H(HCHO)_nHCO$). When during the chemical reduction of glucose the aldehyde group (O=CH-) is replaced with hydroxyl (–OH) group, sugar alcohols are obtained. Sugar alcohols are also called polyol, glycol, or poly Alcohol. Depending on the chemical reduction of sugar, varieties of sugar alcohols are produced. Most frequently used sugar alcohols are mannitol, dulcitol, mailtol, glycol, glycerol etc.

Some of these are obtained from monosaccharide and some are obtained from disaccharides[95].

In this research, sorbitol is used to embed the gold nanoparticles of different shapes and sizes. The sorbitol- AuNPs composite was then utilized to measure the influence of the particle structure and properties on the properties of Au-sorbitol composite.

Sorbitol is found naturally in many fruits and vegetables. It can also be obtained by the hydrogenation of glucose[95]. It is hygroscopic in nature, biocompatible, and environment friendly. Also it is easily available and is cheap. Some of the physical properties of sorbitol are given in TABLE III.

TABLE III. Physical properties of sorbitol[95]

| Properties of Sorbitol | |
|---|---|
| Structure | Linear chain |
| Molecular Formula | $C_6H_{14}O_6$ |
| Melting Point | 95°C |
| Boiling point | 296°C |
| Density | $1.489 gcm^{-3}$ |
| Color | White |

**3.4.** Sample Preparation

Sorbitol D from Sigma Aldrich was taken for making the sample. Aqueous solution of sorbitol D was heated at 120$^{o}$C for 72 hrs in furnace. The 0.2ml colloidal particles were than mixed in 13ml of heated sorbitol. The mixture is than mixed in the 3D mixer at a high speed for 20 minutes. It is then put in vacuum for 12 hrs at 45-50$^{o}$C for removal of gas. The sample is then let to solidify at room temperature. The sample was then ground using SiC sand papers and polished using a polishing pad. The pad was the Polytex fiber-enhanced polyethylene. All samples made were of the same size (1.25' diameter and 8mm thickness) and had flat parallel faces with accuracy of few microns per mm. Due to the perfect cylindrical shape of plastic mold the surface finish was good on the sides. After vacuuming the sample seemed to have no pores nor cracks, and other visible defects. The distribution of Au NPs seems to be uniform in the sample, as it was pink in color showing no aggregates formed.

In the next chapter we will discuss about all the experimental methods used in this work to measure the properties of Au colloid and Au-sorbitol composite.

# CHAPTER IV

# EXPERIMENTAL TECHNIQUES

This chapter deals with the material structure, surface characterization tool, and the experimental procedures. The mechanical properties of nanocomposite (AuNPs-sorbitol) and Au colloid of different shapes and sizes are evaluated.

## **4.1.** X-ray Photo Spectroscopy (XPS)

The XPS is one of the most available surface analysis techniques to characterize surface properties. It uses photon electrons or ions to excite the emission of photons, electrons, or ions from the sample surface. The energy of emissions is then recorded through a high resolution electron spectrometer. The energy spectrum of these emissions provides the information about the elements presented on the sample surface. Since each electron in each atom has a characteristic binding energy associated with that electron, each peak of XPS spectra gives information of the particular orbital of the electron in a particular atom. Mostly a low intensity X-ray is used in XPS. The surface analysis is done under vacuum to avoid contamination of cleaned surface of samples. XPS provides sampling depth of only 10nm [96]. Surface analysis of AuNPs - sorbitol composite was done using the XPS to determine the elemental composition of the sample. Figure 4.1 illustrates the schematic of the XPS. An X-ray of energy ($h\upsilon$) striking an atom ($E_i$), increasing the energy ($E_i + h\upsilon$). The atom releases electron ($E_{K.E}$) and becomes an ion ($E_f$). The difference in the initial energy of atom ($E_i$) and the final energy of ion ($E_f$) is the binding energy ($E_b$) of that particular electron.

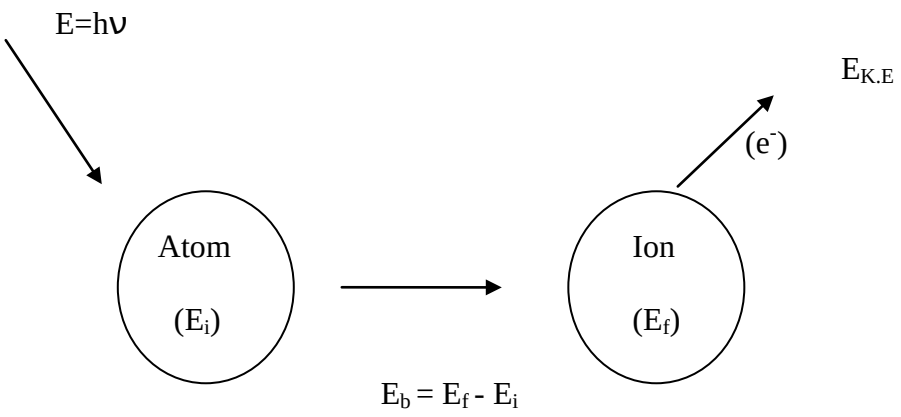


FIG. 4.1. Schematic of XPS

**4.2.** X-ray Diffraction Technique (XRD)

The X-ray diffraction technique, as the name implies, uses X-rays and the diffraction phenomenon to analyze surfaces. This technique is used to get information about the crystalline structure of solids. It is also used to provide the information of three dimensional structures of bio-molecules. After the discovery of X-rays in 1895, Bragg proposed the diffraction pattern theory to get the information of crystalline structure of solids[97].With the current advanced technology; it is possible to figure out the lattice structure using the technique.

During the XRD, a beam of X-ray smacks an atom which increases the energy of electrons. These electrons then produce secondary waves. Some of these waves in certain direction produce constructive interference (as shown in Figure 4.2). This constructive interference in the crystalline structure was defined by Bragg, who derived a simple mathematical relation, given here as equation (4.1):

$$2d\sin\theta = n\lambda \qquad (4.1)$$

*d'* is the distance between planes of atoms in crystalline structure that gives diffraction peak at some '*θ'*, '*θ'* is the angle of incoming X-ray beam that has a wavelength ''*λ'*; and '*n'* is an integer. Here wavelength *λ* is approximately the same as the spacing *d* between planes in the crystal. This X-ray wave interference is called 'X-ray diffraction (XRD)'. We used the XRD to study the crystalline structure of gold nanoparticles embedded in the sorbitol matrix.

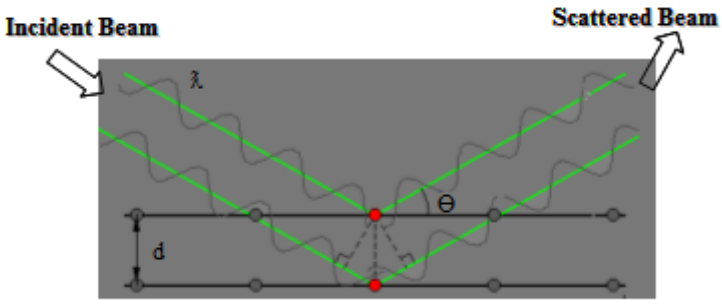


FIG. 4.2. Schematic of XRD

**4.3.** Atomic Force Microscopy (AFM)

The theory of AFM was presented in1986 by Binnig, Quate, and Gerber[3]. The motivation was to overcome the limitation of the STM. The STM can only test electrically conductive or semi-conductive materials. An AFM can image any type of material surface. The first commercial AFM utilized a diamond tip attached to a gold

strip. When the diamond tip reached near the surface, the van der waals forces represented the interaction between the two materials. At that time the vertical movement of gold strip was recorded by a second strip[3,98].

Modern AFM mostly uses a laser beam deflection arrangement[1, 2, 3.] A position sensor is used to spot the location of an AFM cantilever through the reflection of the laser beam from the top of cantilever. Mostly the size of AFM tips is less than 10 nanometers. The cantilevers and tips are made of Si or $Si_3N_4$. A schematic of AFM is shown in Figure 1.5.

An AFM is also used to provide the morphological observation and the electrical conductivity of materials. An AFM is a proficient tool for nanoparticle's characterization. It was discussed in Chapter I that an AFM is also used to evaluate the mechanical properties of nanoparticles. AFM has the ability of producing 3D images, providing information of size, morphology, surface texture, and roughness. The magnification provided by an AFM is as high as 1,000,000x. It also measures the size and surface areas. The volume dispersion of the nanoparticles can be obtained using an AFM, through the height and phase images. In addition, an AFM has the advantages of working in different medium, e.g., air, controlled environment, and in liquid[3,98].

**4.4.** Resonant Ultrasound Spectroscopy

Resonant Ultrasound Spectroscope (RUS) (Quasar International, Albuquerque, NM) is used here to determine the elastic moduli of AuNPs - sorbitol composite[99]. The RUS is a technique where the resonance spectrum of any object can be obtained using ultrasonic waves. This dynamic technique is based on measuring the eigen modes of any object

with a well defined geometry. Since the resonant spectrum of an object depends on its shape, size, elastic constants, density and dissipation, this technique can provide the complete elastic tensor of the object from single resonant spectrum. After the spectrum is obtained, software is used to calculate the elastic tensor of that object. As compare to other ultrasonic techniques (e.g. Pulse Echo Technique) RUS can provide the complete elastic tensor of an object simultaneously along with high accuracy[100].

Originally this technique was used in Geophysics[101]. Almost forty years ago the same technique was first used in material science [101]. The approach was based on one transducer, responsible for sending ultrasonic waves and receiving the resulting signal from sample. A homogenous material was used. The sample of that material had a definite spherical shape. The resonant frequencies of that sphere were measured through RUS. Using the resonant spectra and the analytical methods the elastic properties of that material were calculated. After a few years a two transducer set up was developed [101] where the sample was held between the transducers. One transducer was responsible for sending the ultrasonic wave and the other was to detect the output signal from the sample.

The experimental setup of RUS used in this experiment consists of three piezoelectric transducers, arranged like a tripod[99], Figure 4.3. A disk sample of AuNPs-sorbitol composite was placed on this tripod. One transducer is used to transmit an elastic wave to the sample. In this method the amplitude of this wave is kept steady but the frequency is varied. The other transducers sense the frequency response of the sample. The resonance spectrum obtained through using RUS can be used to determine

the elastic constants. A theoretical frequency spectrum is obtained through preselected elastic moduli of a material along with its dimension and density. Software, consisting of multi dimensional algorithm, is used to reduce the RMS error between the experimental and the theoretical resonance frequencies. After calculating the resonance spectra, elastic constant of the material can then be obtained through the same software.

The accuracy of the RUS method depends on the number of resonance frequencies measured and the quality of the sample. The material should not have any pores or cracks to get accurate results from this technique. Most samples are in shapes of rectangular parallelepiped, cylindrical, and spherical[100].

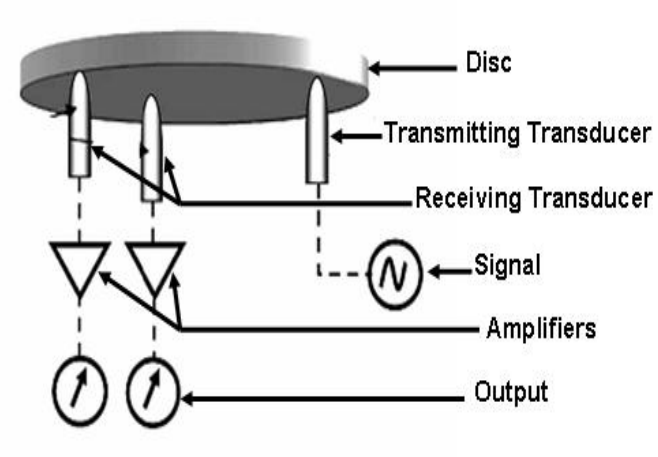


FIG. 4.3. Schematic of RUS[102]

**4.5.** Three-Point Bending Test

In this work the, the bending strength of the AuNPs-sorbitol composite will be measured through a Three Point Bending test. The three-point-bending test is mostly

done for brittle materials since the tensile test is usually difficult for brittle materials. The flexural modulus and stress and strain can be obtained using this method. The biggest advantage of this method is that the preparation of sample is easy. Either rectangular or circular shaped samples (in the cross-section) are used. To obtain reliable results, the dimensions of the specimen need to be consistent throughout the sample[38-40]. In this study the specimen (a rod of uniform cross section Ø=0.5inches) rests on two supports like an overhanging beam, Figure 4.4. The vertical load 'F' is gradually applied at the mid span (L=2inches) and the data is recorded through strain gauge. The data of applied force and the deflection in the mid span of rod are used to calculate the flexural modulus of the material.

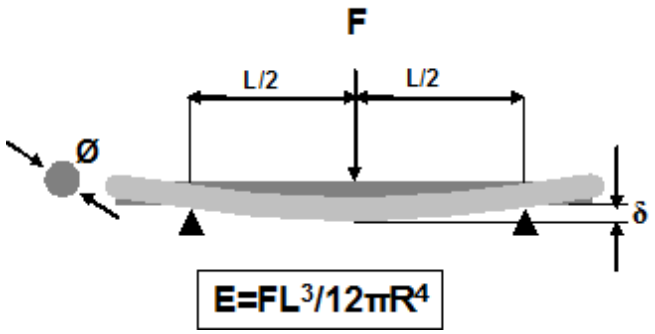


FIG. 4.4. Schematic of three point bending test

**4.6.** Rheometer

In this research an AR-G2 Rheometer (TA Instrument) is used to study the behavior of Au colloid, as shown in Figure 4.5. Rheometer is an equipemt that has the

ability to measure the rheology of fluid under applied stress. During testing a dynamic or static shear strain is applied to the fluid sample and the transducer measures the resultant torque. The other properties can then be calculated using the torque data obtained. In this work Rheometer with parallel plate arrangement is used, as shown in the Figure 1.7. The fluid (Au colloid) is held between two plates. The upper plate moves at an angular velocity (0.1 to 150 radian per second in this work) while the bottom plate is stationary. The temperature of the system ($25^{o}$C) is controlled through the bottom plate.

The Rheometer is used to measure different properties of fluid like, yield stress, shear modulus, creep, viscosity, kinetic property, etc. For nanoparticles suspended in liquid, the Rheometer is a good instrument to evaluate the effects of particles on fluid properties.


FIG. 4.5. An AR-G2 rheometer (TA Instrument)

# CHAPTER V

# EXPERIMENTAL RESULTS

As mentioned in Chapter I, gold at nanoscale was reported to have exceptional properties as compared to other metallic materials at such a small scale. It was also discussed that precise evaluation of mechanical properties of nanoparticles would lead to better understanding of such materials at the same scale. In this work, the sorbitol-AuNPs composite was studied to evaluate shape and size effects of AuNPs on the mechanical properties of the AuNPs- sorbitol composite, using the RUS technique. To further understand this, a Rheometer was used to study the shear properties of Au colloid. The XRD analysis was done to determine the crystal structure of the composite. An AFM was utilized to characterize the phases and their properties, present on the surface of the samples. This chapter reports all experimental results in detail.

## **5.1.** Elemental Composition of AuNPs-Sorbitol Composite Using XPS

Surface analysis of AuNPs-sorbitol composite was done using XPS, to determine the elemental composition. Figure 5.1.A. and Figure 5.1.B, show the spectra obtained for 55 nm AuNPs-sorbitol composite at low and high concentrations (TABLE III) of AuNPs in composite. For comparison, the spectra obtained for Au colloid is also shown in Figure 5.2.

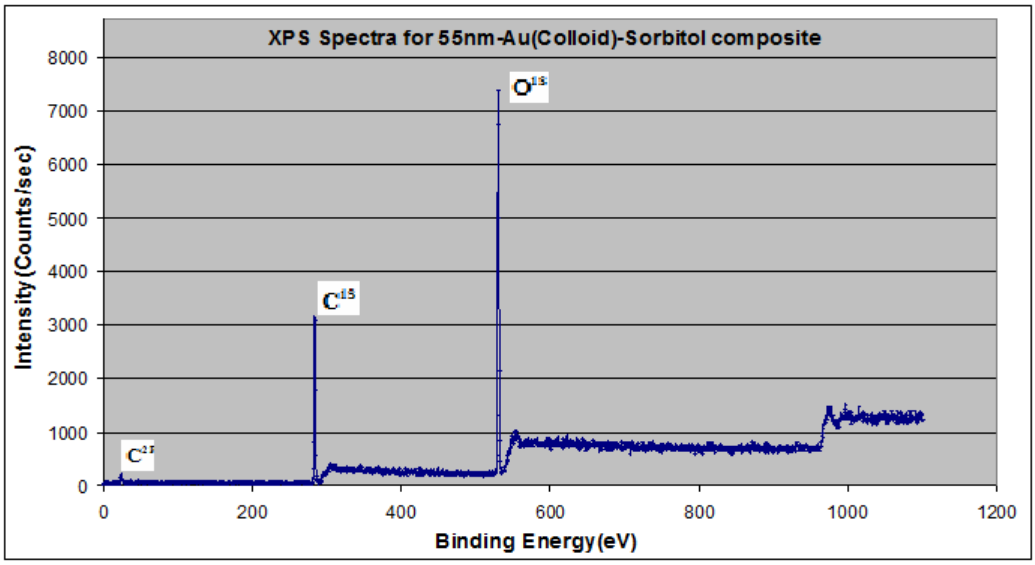


FIG. 5.1.A. XPS result for Au (nanosphere)-sorbitol composite at low concentration

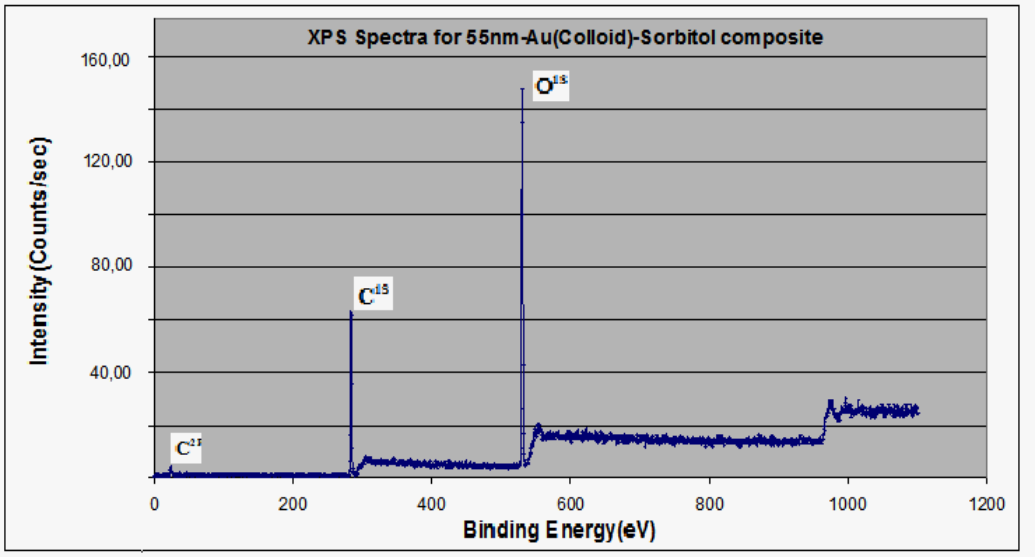


FIG. 5.1.B. XPS result for Au (nanosphere)-sorbitol composite at high concentration

Figure 5.1.A and Figure 5.1.B clearly show XPS spectra of Au-sorbitol composite of $C^{1S}$ and $O^{1S}$ peaks. No Au peaks found at either concentration. In order to

detect the effects of interfacial interactions between Au and matrix molecules, a sample of AuNPs colloid was analyzed using the XPS, as shown in the Figure 5.2. It is seen that there is a small peak of gold. The fact that AuNPs were not shown in the solid composite and were seen in the colloid indicates that the sorbitol molecules hindered the AuNPs by wrapping around them. Details will be discussed later.

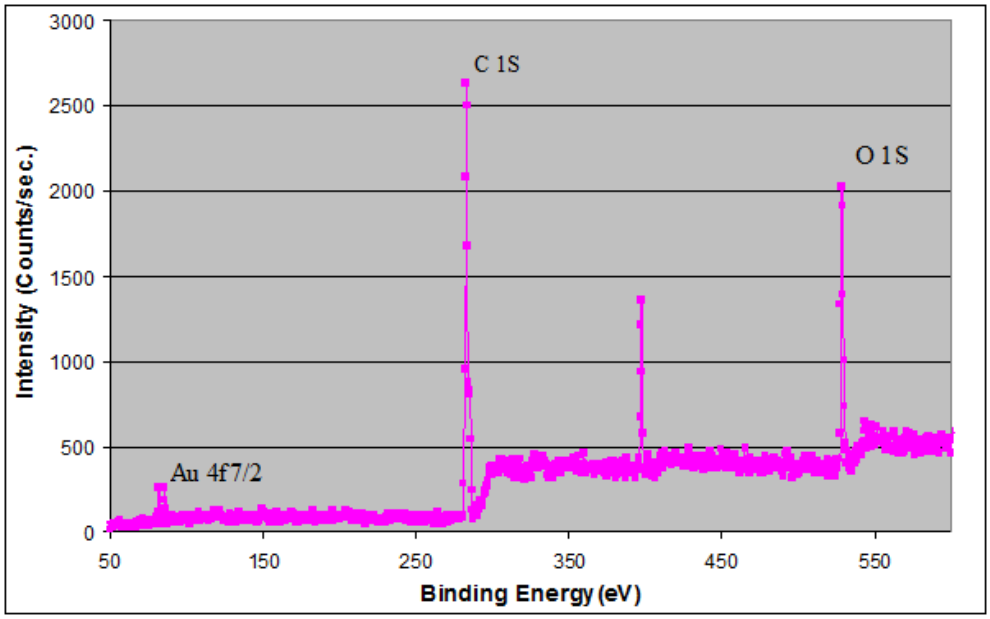


FIG. 5.2. XPS result for Au colloid

**5.2.** Crystal Structure of Gold Nanoparticles Using XRD

To determine the change in the crystal structure of Au NPs, the XRD test was conducted for the Au-sorbitol composite**.** Figure 5.3 shows the XRD spectra of Au-sorbitol composite of different diameters of Au nanospheres.

**XRD Spectra of Au (Nanospheres)-Sorbitol Composite**

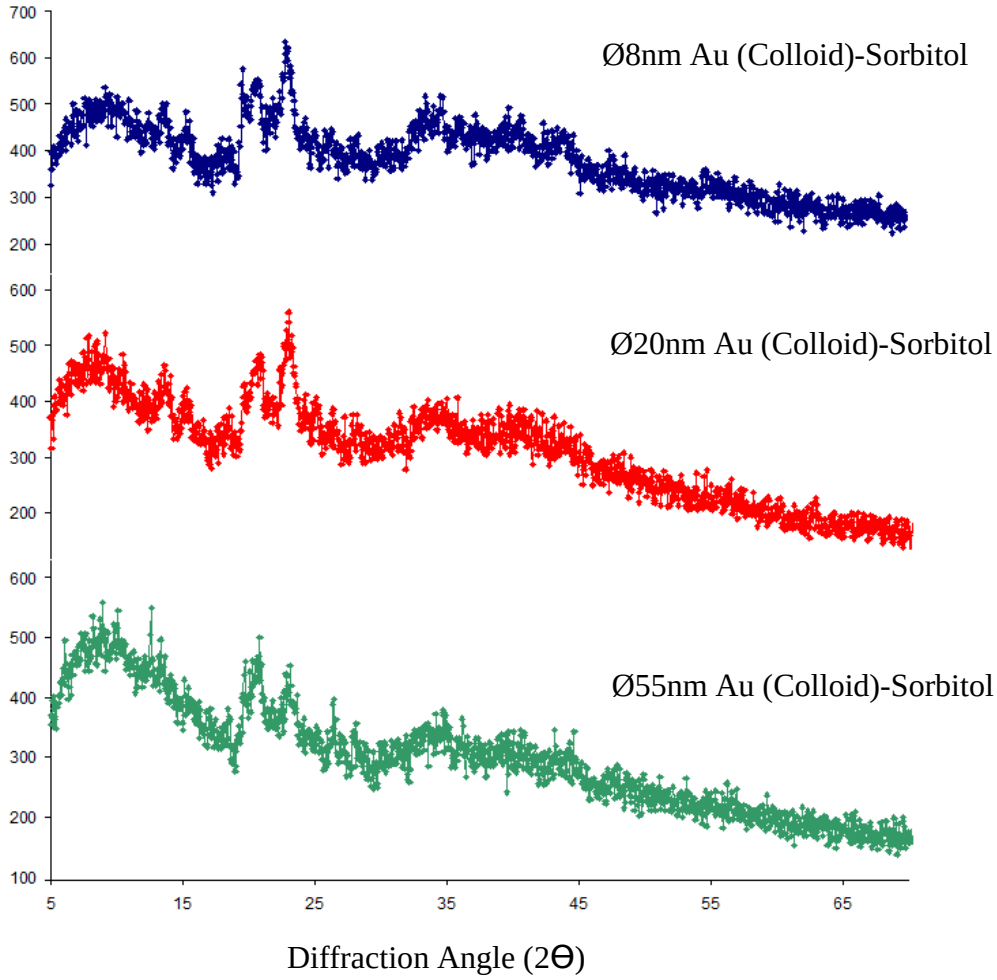


FIG. 5.3. XRD spectra of Au-sorbitol composite for different Au nanospheres

As shown in Figure 5.3, there was no visible change in peaks due to different sizes of Au-spheres in the AuNPs-sorbitol composite. There was no Au peaks found in the XRD spectra.

The rod shaped Au colloid was further analyzed in order to compare the nanospheres and nanorods. Figure 5.4 shows the XRD spectrum of Au (nanorods)-sorbitol composite.

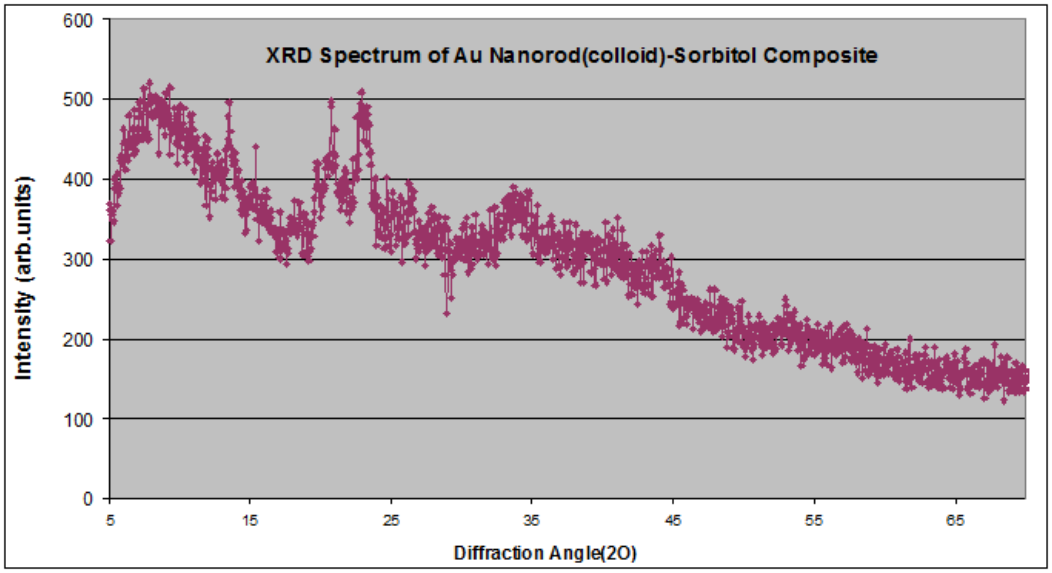


FIG. 5.4. XRD spectrum of Au (nanorods)-sorbitol composite

Comparing Figure 5.3 and Figure 5.4, no difference was found in the Au (nanorods)-sorbitol composite. It is possible that the Au NPs are fully covered by sorbitol and cannot be detected by using the XPS or XRD. The mechanisms will be discussed later.

## **5.3.** Topography of Au- Sorbitol Composite Using AFM

To study the topography of the Au-Sorbitol composite, an AFM was used. The images of the sample surfaces were taken using the close-contact mode of the AFM.

### **5.3.1.** Effects of Au Nanosphere Size

The value of average surface roughness on the surfaces of composites and sorbitol is plotted and shown in Figure 5.5. Figures 5.6(A-D), shown below, are the phase (right) and the height (left) images of the sorbitol, and its composite at low concentrations of Au. Figures 5.6.B-D, give the phase and height images of different sizes of Au nanospheres. Both phase and height images change with variation in the size of nanosphere. Surface of the material seems to be very smooth. The value of surface roughness is decreasing with the increase in the size of particle. Unlike the AuNPs of Ø8nm and Ø55nm, the addition of Ø20nm Au did not affect surface roughness value of the sorbitol.

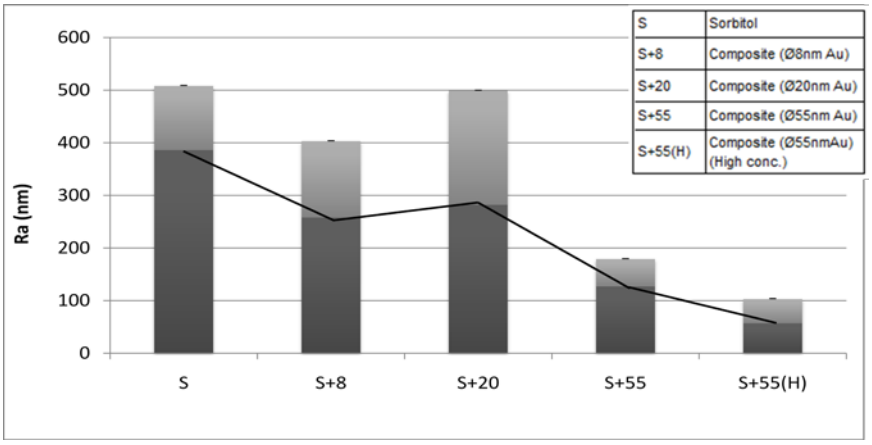


FIG. 5.5. Error bar graph and trend line showing the effect of Au NPs size on the average roughness of sorbitol

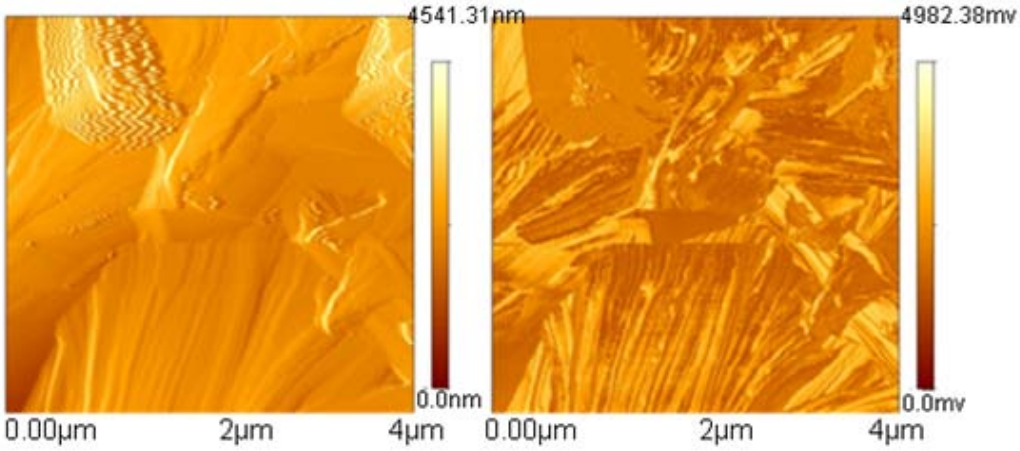


FIG. 5.6.A. Phase image (right) and height image (left) of sorbitol (scan range 4µm x 4µm)

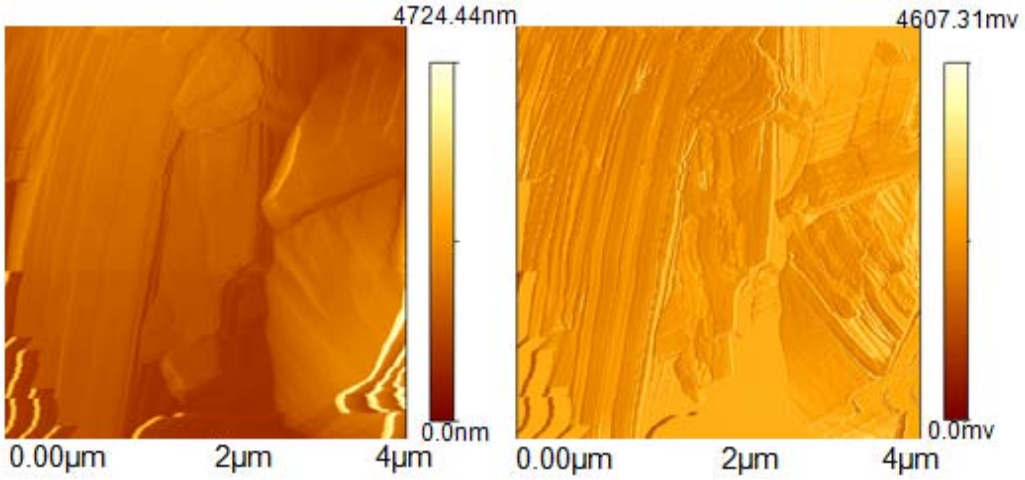


FIG. 5.6.B. Phase image (right) and height image (left) of sorbitol- Ø8nm Au (scan range 4µm x 4µm)

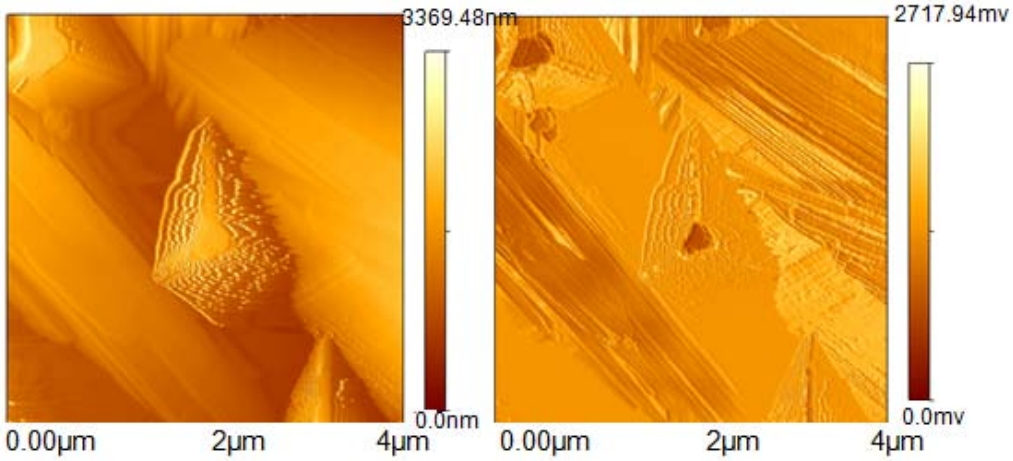


FIG. 5.6.C. Phase image (right) and height image (left) of sorbitol- Ø 20nm Au (scan range 4µm x 4µm)

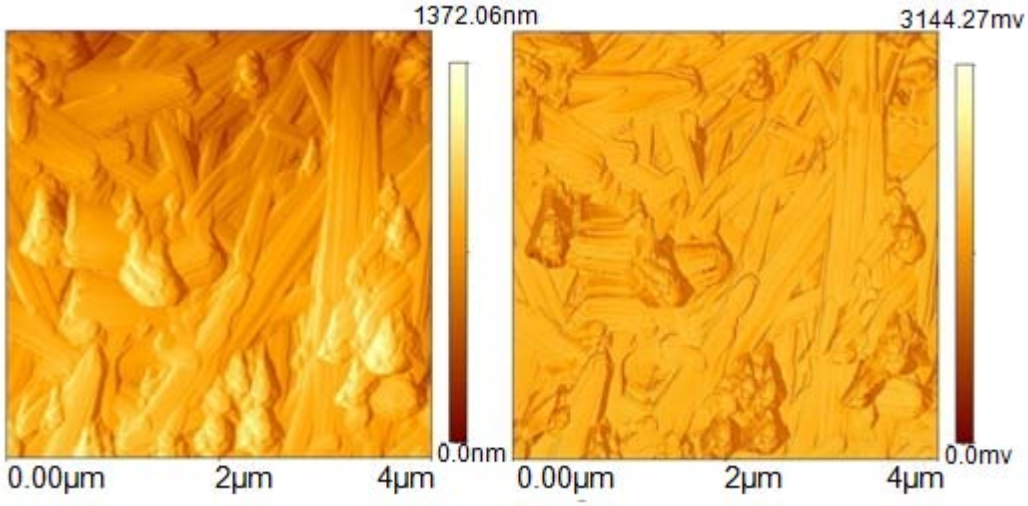


FIG. 5.6.D. Phase image (right) and height image (left) of sorbitol- Ø 55nm Au, (scan range 4µm x 4µm)

### 5.3.2. Effects of Au Nanosphere Concentration

The image of the composite with high concentration of Ø55nm Au is shown in Figure 5.6.E. The images are significantly different from that in Figure 5.6.D, where low concentration of Ø55nm Au is used. In Figure 5.6.E, there are clear signs of grains formed. The higher magnification in Figure 5.6.F, shows these grains more clearly. The value of roughness decreased with the AuNPs concentration.

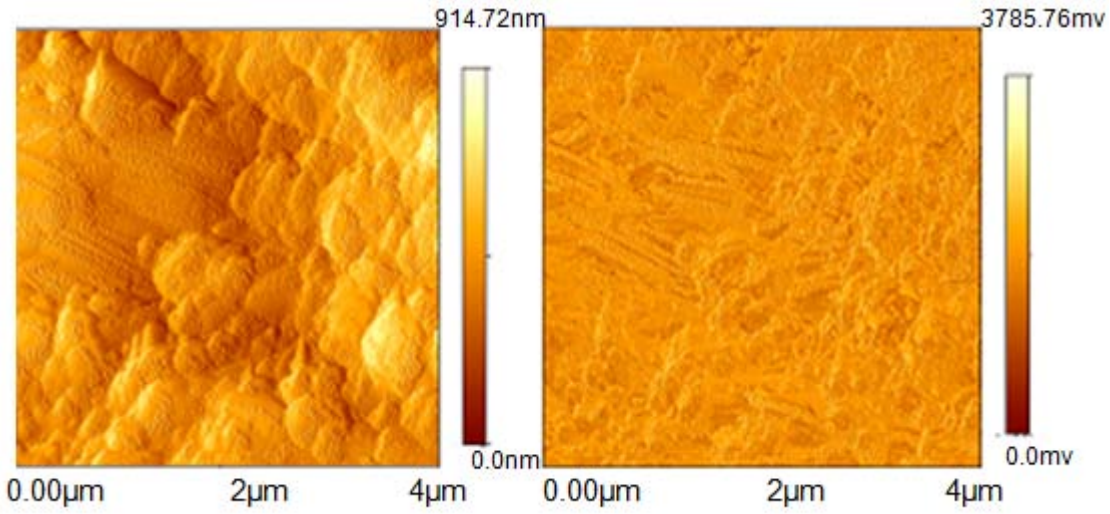


FIG. 5.6.E. Phase image (right) and height image (left) of sorbitol- Ø 55nmAu (high concentration), (scan range 4µm x 4µm)

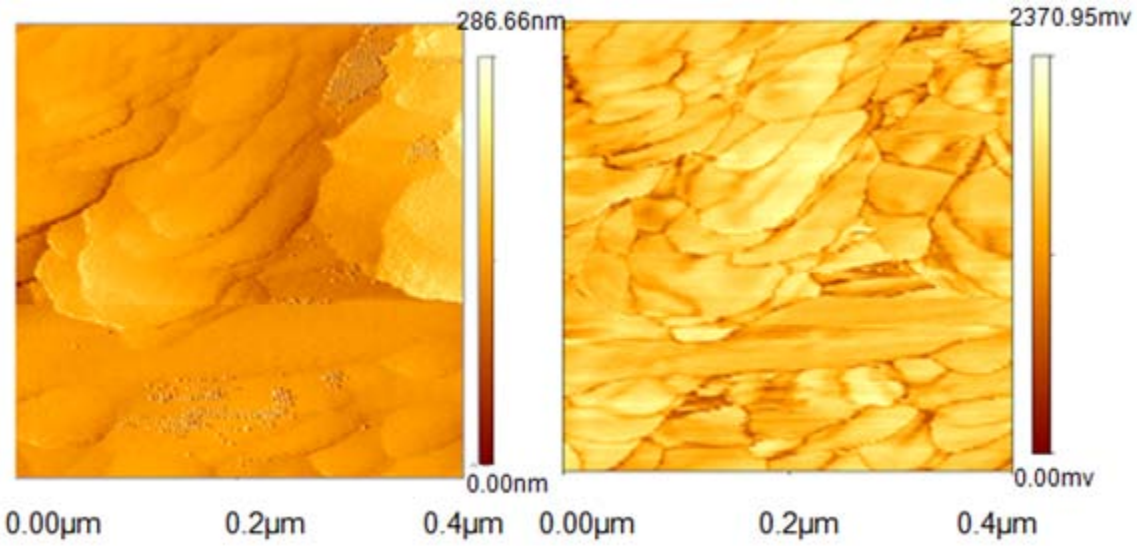


FIG. 5.6.F. Phase image (right) and height image (left) of sorbitol- Ø 55nm Au (high concentration), (scan range 0.4µm x 4µm)

### 5.3.3. Effects of Au Nanorod

To see the effects of shape on the morphology of composite, Au nanorods (Ø40 nm, L=300nm) are used, as shown Figure 5.6.G. Comparison of Figure 5.6.B-F, with the images of Figure 5.6.G, shows that the effect of shape is apparent, considering the difference in the potential of surfaces. The phase image of nanorod composite seems to have only one phase present in the images.

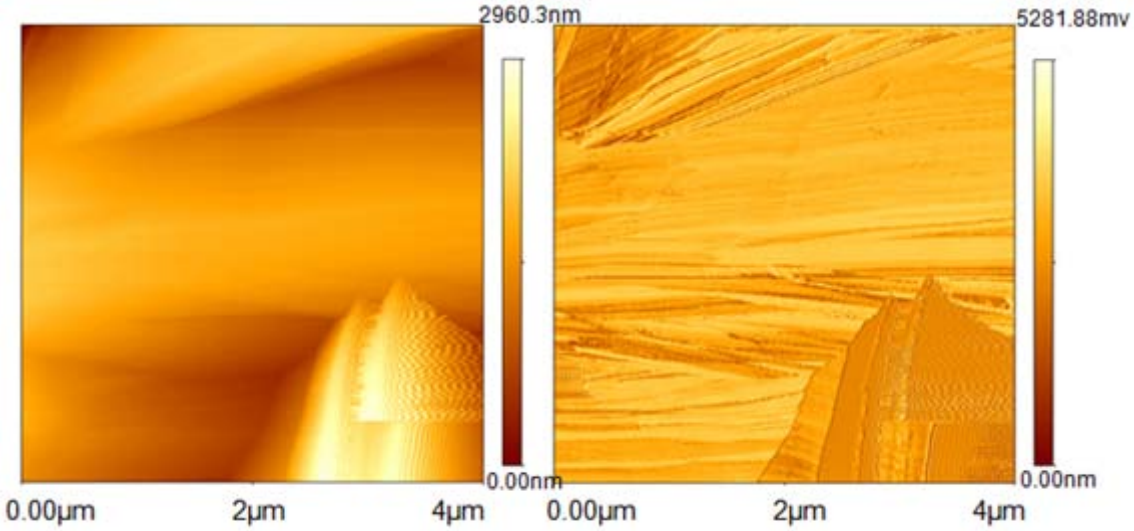


FIG. 5.6.G. Phase image (right) and height image (left) of sorbitol- Ø40nm Au rods (scan range 4µm x 4µm)

**5.4.** Adhesion Force Measurement on Au- Sorbitol Composite Using AFM

The adhesion forces were measured on the sample. A silicon probe of diameter less then 10nm was used. The stiffness of AFM cantilever beam used was 0.2nN/nm. The experiments were repeated three times at three different locations. Curves are shown in Figures 5.7.A-B as typical ones. The data is plotted in Figure 5.7.C. The trend line and the standard deviation are showing the consistency of the measurements.

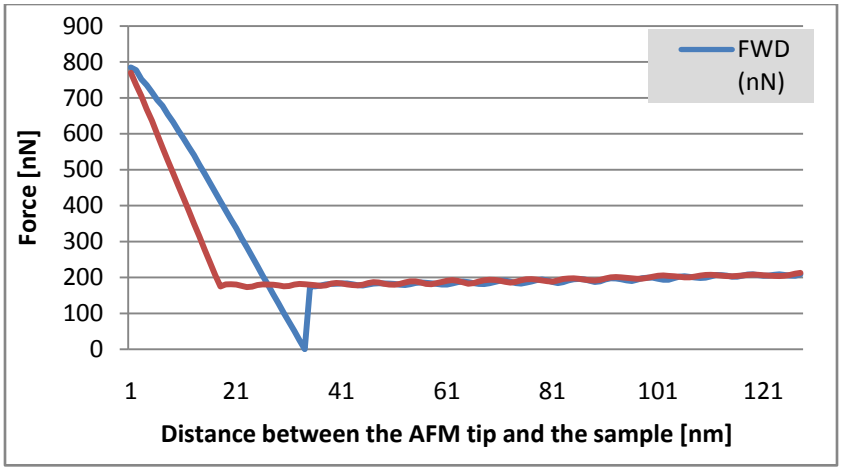


FIG. 5.7.A. Force distance curve for low concentration Ø55nm Au-sorbitol composite

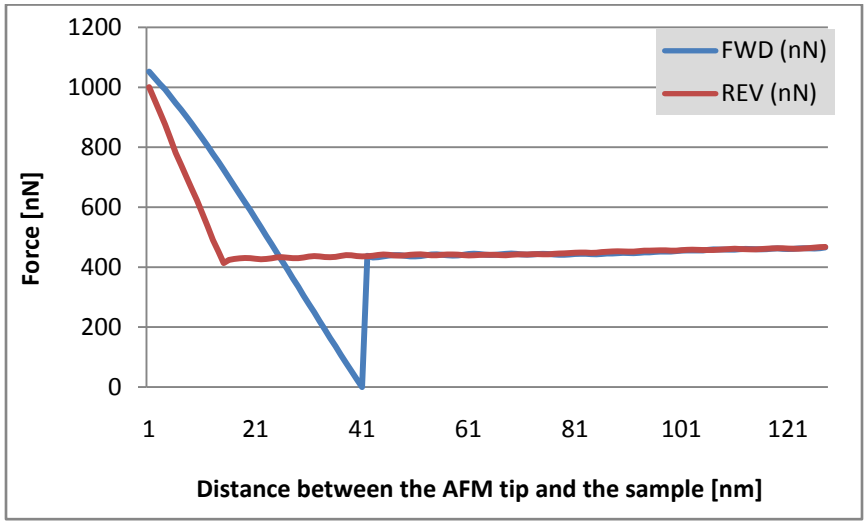


.

FIG. 5.7.B. Force distance curve for high concentration Ø55nm Au-sorbitol composite

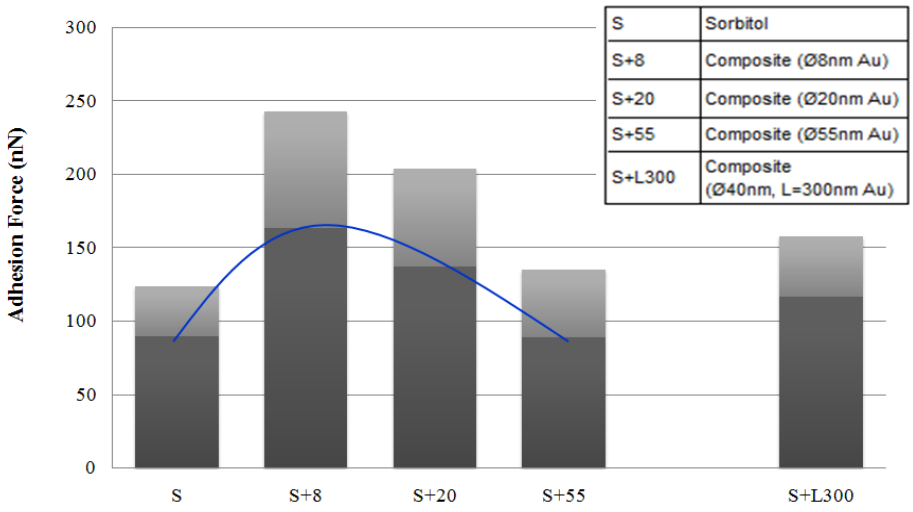


FIG. 5.7.C. Error bar graph and trend line showing the effect of Au NPs on the adhesion force of sorbitol

The trend of the adhesion force was decreased with the increase in size of Au nanospheres. The increased size of gold nanospheres then started lowering the value of adhesion. This is due to the interactions between the AFM probe and the sample surface molecules. Detailed discussion will be presented in next chapter.

In the next section the results of mechanical properties of Au-sorbitol composite are presented.

## **5.5.** Mechanical Properties of Sorbitol-AuNPs Composite

### **5.5.1.** RUS Results

The Au-sorbitol composite was tested using the RUS, to get the resonance spectra of the material. The resonant frequency of a material is directly related to its elastic properties. This relationship could be exploited to understand the effects of shape and size of NPs on their elastic properties. In Figure 5.8 below, the resonance spectra of different Au-sorbitol composites are given.

The peaks in all spectra fall in the same frequency range. There are no significant peaks shown as those in micro structured ceramics[103].

**RUS Spectra of Au –Sorbitol Composite**

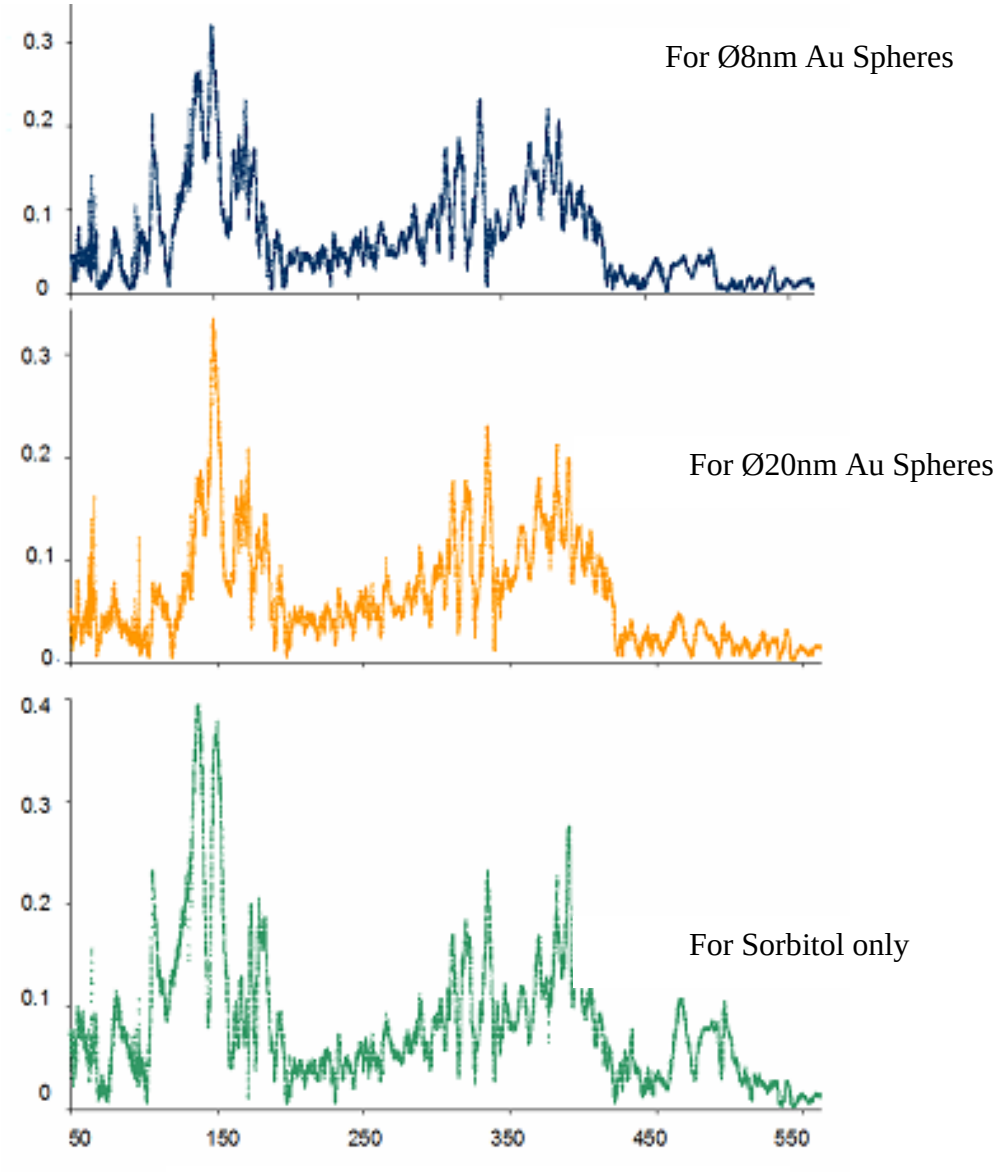


FIG. 5.8. RUS spectra of sorbitol and Au-sorbitol composite

The alumina particles of Ø20μm were then used with Sorbitol to test the particle size limit of RUS. TABLE IV list two different concentrations of alumina used to make

alumina-sorbitol composite. Figure 5.9 shows the RUS spectra of μØ20 alumina - sorbitol composite at low and high concentrations.

TABLE IV. Alumina microsphere (Ø20μm) used in this research

| Concentration | Number of particles | Sample disk size |
|---|---|---|
| 1. Low | $1.39 \times 10^8$ | Ø1.45'(3.68mm), t= 0.31'(8mm) |
| 2. High | $2.08 \times 10^8$ | |

The RUS Spectra of alumina-sorbitol composite showed some peaks at high frequency. A low intensity peak is visible at a frequency of 1060 KHz. Such peaks were not observed at the low concentration. This is different from that in AuNPs. This result indicates that metal microparticles could be detected by the RUS and the AuNPs remain to be a challenge.

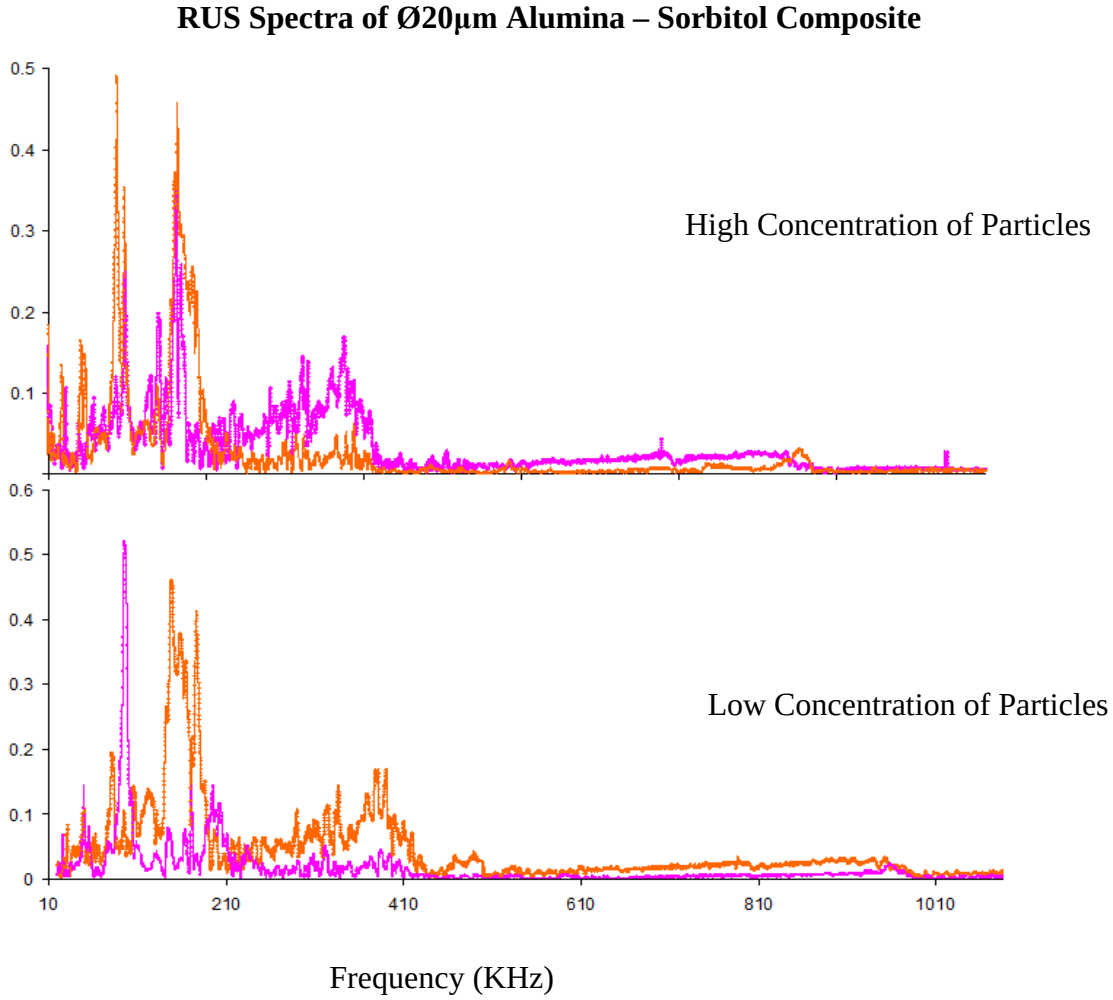


FIG. 5.9. RUS spectra of alumina sorbitol composite

**5.5.2.** Three Point Bending Test for Au-Sorbitol Composite

The bending result was conducted on the tensile testing machine. The bending result of Au-sorbitol composite is shown in the TABLE V. The decrease in the bending stiffness of sorbitol is quite significant with the introduction of nanoparticles. Increased surface area of nanorods, as compare to nanosphere, affected the bending stiffness more significantly. Details will be discussed later.

TABLE V. Three point bending results for Au-sorbitol composite

| Sample | Flexural Modulus |
|---|---|
| Sorbitol only | 0.173 GPa ± 0.03 |
| Sorbitol & gold nanorods (Ø40nm x 300nm) | 0.055 GPa ± 0.015 |
| Sorbitol & gold nanospheres (Ø55nm) | 0.108 GPa ± 0.042 |

**5.6.** Shear Properties of Au Colloid

**5.6.1.** Shear Properties of Spherical Au Colloid

To study the shear properties of Au colloid, nanospheres and nanorods of Au with different sizes were used. An ARG2 Rheometer was used to evaluate the properties of Au colloid. The different properties of Au colloid, such as viscosity, shear stress, and shear rate were determined. The colloid was held between two parallel plates with the upper plate rotating with an angular velocity of 0.1-150 r.p.s. The viscosities of Au colloid were measured at different loads, velocities, and concentration. Figure 5.10.A. shows the average shear stress vs. shear rate measurement for Ø8nm, Ø25nm and Ø75nm spherical Au colloid. Since the sensitivity of the Rheometer in terms of torque is in a few nN.m range[79] the difference shown in results is significant.

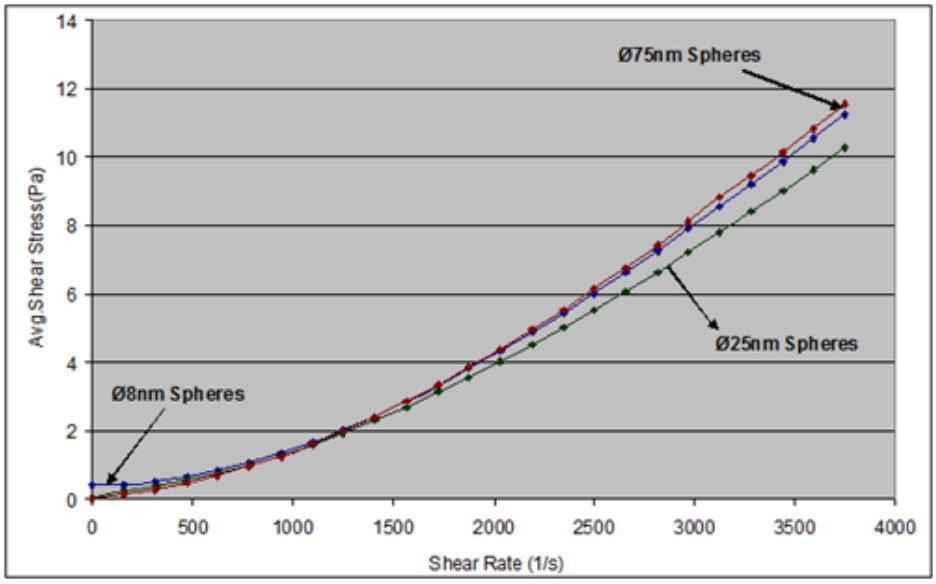


FIG. 5.10.A. Average shear stress vs. shear rate for different spherical Au colloid

In Figure 5.10.A the blue curve shows the behavior of Ø8nm. The red curve is for Ø75nm and the green curve is for Ø25nm Au colloid. It is clear that all three Au colloids provided increased shear stress with increasing shear rate. The behavior of Ø8 nm and Ø75 nm Au colloid are similar. While the shear stressed of Ø25nm and Ø75 nm Au colloids are initially almost the same. After reaching a certain value, 1250 radians/second of shear rate the shear stress increased more in Ø75 nm than that in Ø25nm and Ø8nm colloids. Since all these particles have different surface area, which is considered important in the fluid shear. Details will be discussed in detail in the next chapter. Details will be discussed in detail in the next chapter.

The same gold colloids were found to have different viscous behavior at different shear rate values, Figure 5.10.B. These colloids show non-Newtonian behavior. At low shear rate shear thinning behavior and at high shear rate shear thickening behavior are

observed. All the colloids started thickening at approximately the same shear rate. It is also clear that the Ø75nm Au colloid didn't show any significant difference in viscosity at different shear rates.

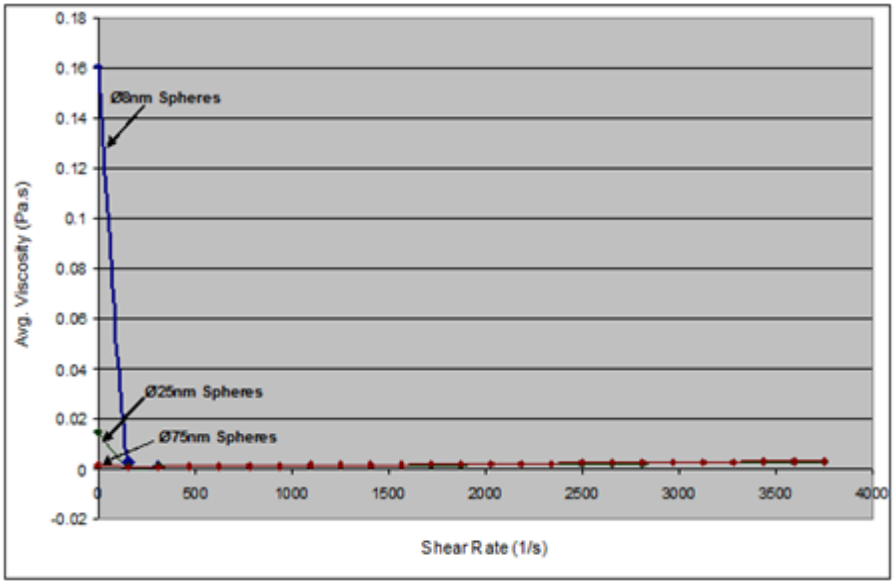


FIG. 5.10.B. Average viscosity vs. shear rate for different spherical Au colloid

Au colloids of different concentrations were also tested and results were compared for viscosity and shear behavior. Figure 5.11.A. and Figure 5.11.B show that concentration does affect both the shear stress and viscosity of the colloid.

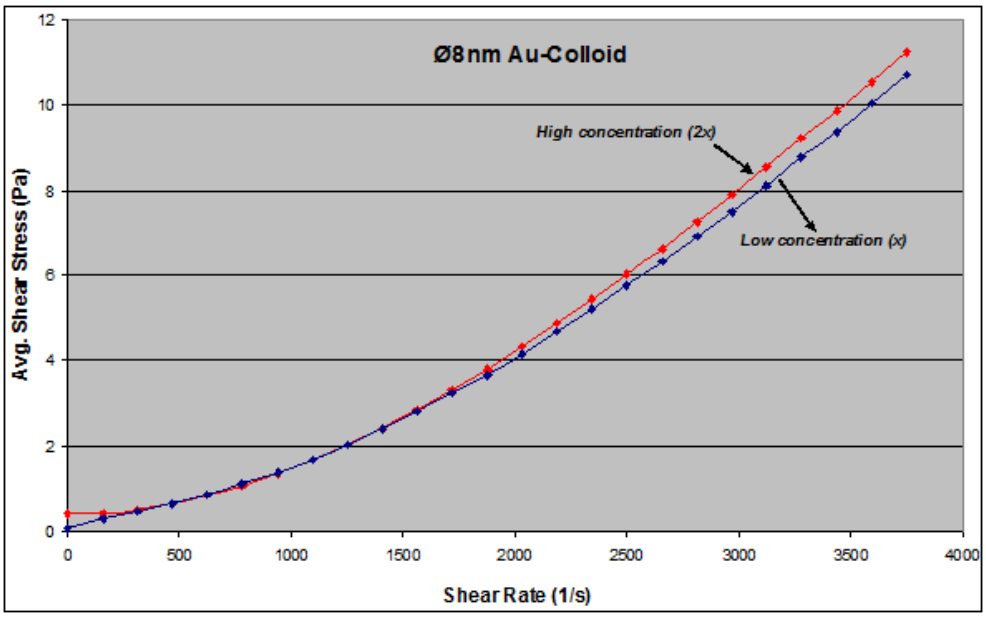


FIG. 5.11.A. Concentration effect of Ø8nm Au-colloid on shear stress

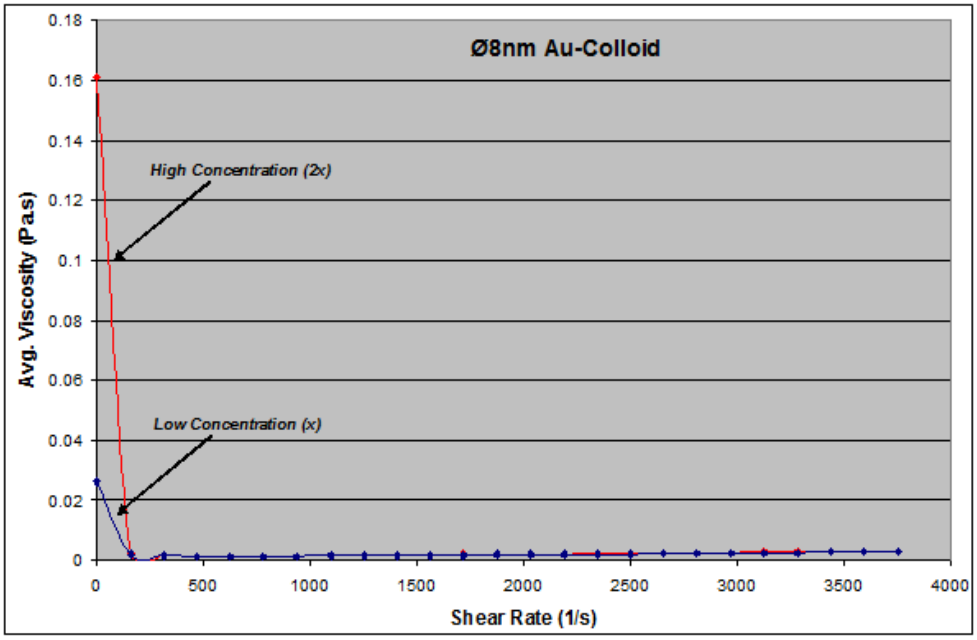


FIG. 5.11.B. Concentration effect of Ø8nm Au-colloid on viscosity

Also it shows that the effect of concentration is significant in colloid of Ø8nm then in Ø25nm Au colloid. The shear and viscosity results of Ø25nm Au colloid are shown in Figure 5.12.A and Figure 5.12.B respectively.

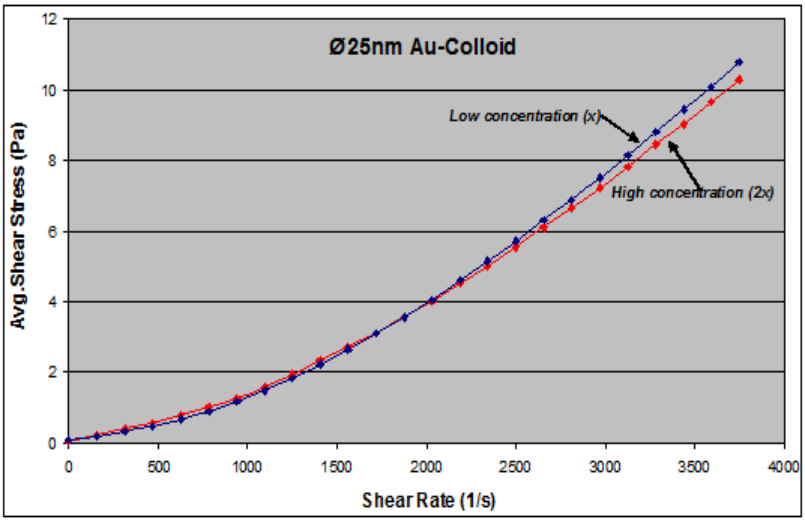


FIG. 5.12.A. Concentration effect of Ø25nm Au-colloid on shear stress

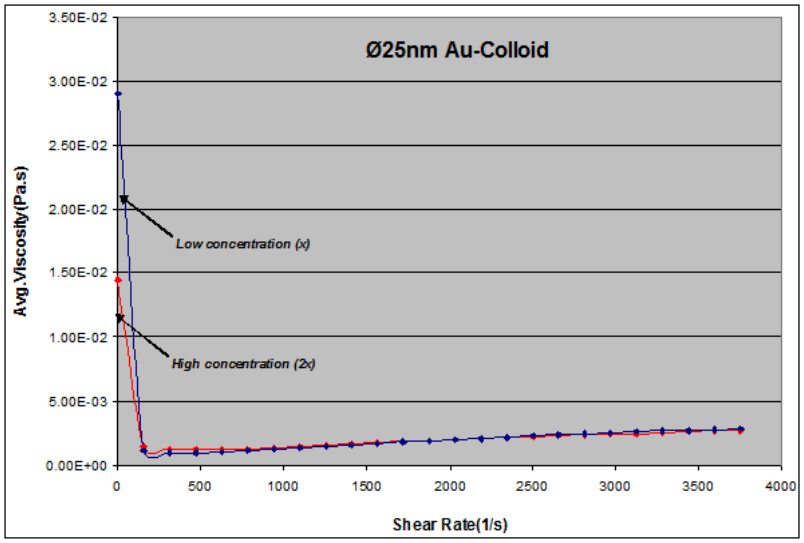


FIG. 5.12.B. Concentration effect of Ø25nm Au-colloid on viscosity

**5.6.2.** Shear Properties Nanorods Au Colloid

Rheology of nanorods colloid of two different sizes was also tested. Figure 5.13.A and Figure 5.13.B show the shear stress and viscosity results of different nanorods. The red curve is for long nanorods (Ø40nm, L=300nm) and the blue curve is for short nanorods (Ø10nm, L=120nm).

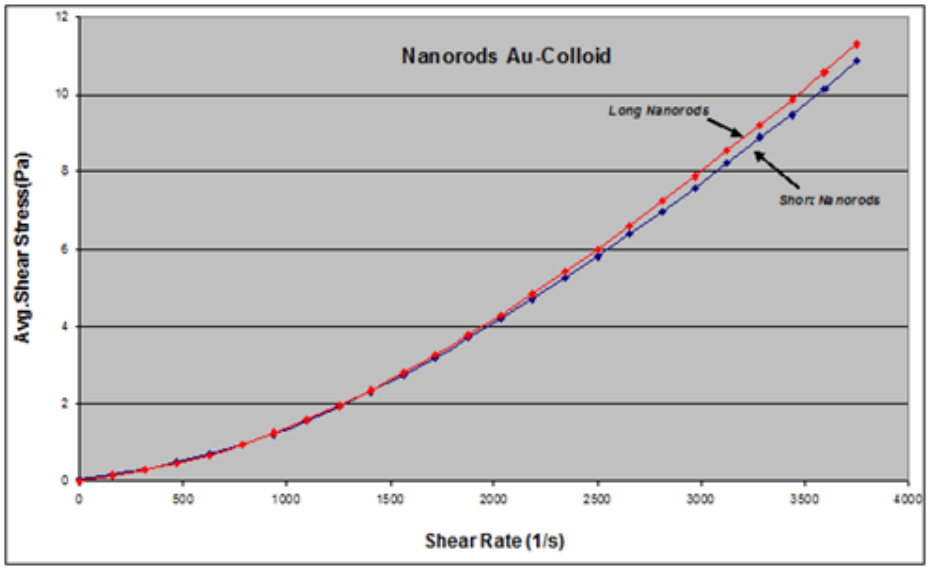


FIG. 5.13.A. Effect of nanorod size on shear stress of Au colloid

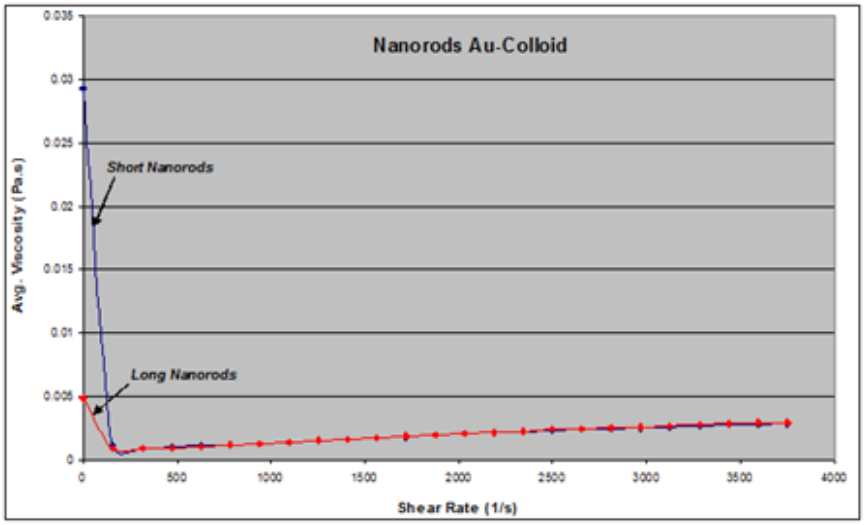


FIG. 5.13.B. Effect of nanorod size on the viscosity of Au colloid

It is found that the size of nanorods does affect the shear behavior of Au colloid. The viscosities of these colloids have significant difference. The behavior of nanorods colloid, in this way is similar to the behavior of nanosphere Au colloids, where surface area of the nanoparticle seems to affect the viscosities and shear stress of Au colloid significantly.

# CHAPTER VI

# PROPERTIES OF GOLD COMPOSITE

This chapter discusses the experimental results presented in Chapter V. The mechanical properties of Au-sorbitol composite are discussed here. The analysis of the results using XPS, and XRD techniques are also given here. The last part covers the mechanisms of rheological behavior and shear properties of Au-colloid.

## **6.1.** Elemental Composition and Structure

As mentioned in the Chapter IV, the XPS is a surface analysis technique with high sensitivity. This technique measures the properties within a few nanometers of the surface material. In chapter V, the XPS spectra obtained for Au-sorbitol composite revealed the presence of ‘C’ and ‘O’ peaks. However, the XPS did not detect gold nanoparticles present in the sample, as shown in Figure 5.1 and Figure 5.2.

The AuNPs-sorbitol composite was also tested to check any change in the crystal structure with change in shape and size of AuNPs. The diffraction spectra obtained using the XRD was shown in Figure 5.3. The XRD did not provide any identifiable peaks. It is clear that there are some visible peaks. These visible peaks are not from gold nanoparticles, as the diffraction angle is not the same as the bulk gold according to the literature[104]. The XRD results of all samples mostly fall in the same region. There is almost no obvious difference between these peaks, as shown in Figure 5.3. Since no difference seems to exist between the spectra of sorbitol with and without particles, it means that gold NPs were not detected by XRD. Furthermore, the XPS did not detect

any peaks from gold NPs. This again proved that the AuNPs were not detectable by the highly sensitive X-rays. This could mostly due to the absorption of X-ray by the sorbitol and there might be a thick layer of sorbitol coating around the AuNPs. The ‘C’ and ‘O’ peaks were seen under the X-ray. The testing depth of XPS is only 10 nanometers; the layer of sorbitol is more than 10 nm. The presence of ‘O’ and ‘C’ can be due to sorbitol. The other reason could be the concentration of NPs. It is possible that if the concentration of NPs is increased substantially the XPS and XRD can give information about the composition and crystal structure of this composite. However, sorbitol is very hygroscopic, only a limited volume of colloid can be mixed in sorbitol. Attempts were made to increase the volume of colloid in sorbitol but it could not be mixed with more than 0.4ml of colloid in 13ml of sorbitol.

**6.2.** Topography and Adhesion Force

The gold colloids capped by the citrate were used for this research (section 5.3). The topography of the sample surface (AuNPs-sorbitol composite) was then examined by using AFM. As shown in Figure 5.6.A, the phase image of the sorbitol shows crystalline material like structure, as sorbitol was crystal. The lines in phase image of sorbitol are oriented. When the 8nm spheres were added, the phase image of the composite showed a different structure (Figure 5.6.B). The surface roughness reduced but the deviation increased, Figure 5.5. Also the size of sorbitol grains are bigger as compare to the size of grains of Ø55nm sphere composite (Figure 5.6.E). The Ø55nm

particle had even a lower value of roughness. The microstructure of this composite is changing with the change in the size of sphere.

When the particles were added in the sorbitol, there could be a possibility that these particles serve as a low temperature site for a higher temperature sorbitol. That gave sorbitol an opportunity to surround the metal surface and solidify. The sorbitol starts becoming thick soon after the temperature drops below $90^{o}$C and it does not let the particles disperse uniformly. The Ø8nm particle is too small to be seen by a scan area of 0.4µm x 0.4µm. Thus the change in the microstructure is not as apparent as in Ø55nm nanosphere. In case of Ø20 nm sphere, the change in microstructure is more apparent than the Ø8nm sphere. The Ø55nm has visible grain structures even at a lower concentration of particle, Figure 5.6.D.

At high concentration the phase image (Figure 5.6.E) shows a grain-like structure of the composite. The size of this structure seems to be quite uniform. The width of this grain like structure is about 60-70 nm, similar to the particle size (Figure 5.6.F). It is possible that instead of forming aggregates, the particles were individually capped by sorbitol. This supports the discussion for the low concentration composite above. With the high concentration of AuNPs, the heat was expected to be transferred more effectively. The nucleation would be increased resulting in a high number of sorbitol grains. It can also be the reason of higher deviation in the average surface roughness of composite with smaller particles.

Figure 5.5 shows the value of roughness of the composite at different concentrations. The materials were soft but there is no scratches seen (Figures 5.6 A-G).

The roughness is higher in the light color region and lowest in the plain dark region. The area of bright color region has increased as compare to dark color region at higher concentration. Details will be given next.

As shown in Figure 5.6, the light color regions are high peaks under an AFM. In the phase image, the light color area is correlated to the high peaks where a phase with different mechanical response to the AFM probes. Potentially, this light area represents a harder phase compared to the dark. This means that the high area is the hard phase that was introduced through chemical reactions during the mixing and the solidification. It was reported that the esterification of sorbitol could be formed at temperatures from 110 to 150$^{o}$C [105]. When the sorbitol was in mix of citric acid or citrate ions, it was polymerized to form esters. The loose citrates ions were likely to exist in the solution. These citrate ions were polymerized with sorbitol and formed ester. This explains the presence of less light color regions as compare to the darker region in Figure 5.6.D of low concentration of colloid. In the high concentration sample, the lighter color region had increased when more colloid was mixed in sorbitol (Figure 5.6.F). The dark color area in the phase image seemed to be the sorbitol covering the citrate capped gold nanoparticles. No visible sign of gold nanoparticles appeared to be on surface in Figures 5.6.A-D.

This and previous session indicate that the surface chemistry of Au-colloid sorbitol composite might have affected the surface morphology. To evaluate the effect of the surface chemistry on the adhesion characteristic of the surface, an AFM is used for further analysis.

Adhesion is the binding of two molecules due to the attractive forces that exist between them. When two surfaces come in contact, the difference in the surface chemistry can cause adhesion. In this experiment the gold nanoparticles seems to be completely covered with the sorbitol. The local adhesion property of this organic material coating is measured through an AFM.

The mean value of the adhesion force with deviation is given in Figure 5.7.C. The deviation is very high and the mean value decreases with the increased size of gold spheres. The concentration affected the adhesion force. Figure 5.7.A & Figure 5.7.B show that the adhesion force increased significantly when the concentration of Au colloid was increased. The measured adhesion force is the attraction force, linking the molecules on the tip of AFM and those on the surface of the composite. In general, the adhesion force is the sum of van der Walls forces, electrostatic forces, capillary forces, and forces due to chemical bonding. Sorbitol is found to be hygroscopic at the room temperature[106]. Thus, the possibility of contribution of capillary force in adhesion is bleak. However, the van der waal forces of attraction are always present. The conductivity measurement using a Kevin probe of the AFM showed that there was not any measurement bear of AuNPs on the surface (results are not shown). This means that the chance to directly measure the adhesion between AuNPs and the AFM probe is not likely. The remaining reason would the softening of the sorbitol due to addition of AuNPs solution. The high deviation seems to be due to the presence of two different phases.

**6.3.** Mechanical Properties

The three point bending test results (TABLE V) showed significant effects of the addition of gold nanoparticles. This is also evident from the fact that by increasing the surface area of the NPs the effects becomes more pronounced. The plot of the surface area vs. the particle diameter is given in Figure 6.1.

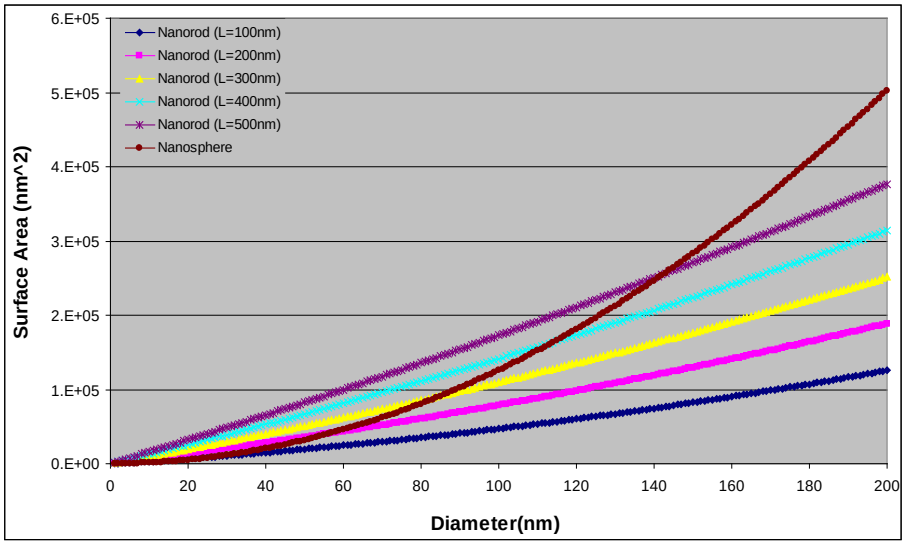


FIG. 6.1. Comparison of the surface area of rod & sphere

In case of spheres, there is a parabolic relation of the surface area verses the size of the diameter. In case of nanorods, a close-to-linear relationship is found. In this work the sphere has a diameter of Ø55 nm and the surface area is much less than a Ø100 nm long rod of same diameter. At the same volume of sphere and rod as mentioned in Chapter III, a sphere will have a lower value of surface area. Generally, in the composite, the increased surface area results in the increase in the contact area, i.e., the

interfacial interactions. Surface chemistry of both materials defines the interfacial forces. The decrease in the flexural modulus with increase in the interfacial area can be the due to the weakening of the interfaces through shrinkage of sorbitol during solidification. The shrinkage of the sorbitol formed a gap between the particle and the sorbitol. These weakened interfaces resulted in the decrease of bending stiffness of the composite.

To observe the effects of size and shape of NPs on the other mechanical properties of this composite, the RUS tests were conducted. The resonant spectra of different size and shape of AuNPs-sorbitol composite were obtained using the RUS and were compared in Figure 5.8. The spectra of any metallic material are expected to show visible peaks at the resonant frequency. Comparing the resonant spectra of AuNPs-sorbitol composite with that of sorbitol only (Figure 5.8), samples showed that the peaks of composites cannot be differentiated from that of sorbitol. Discussions about this are as follows.

The ultrasounds velocity in solids depends on the elastic modulus and the density of the material. For a longitudinal wave in a solid medium the velocity is given by the relation[107]

$$C^l=\sqrt{[E(1-\nu)/\rho(1-\nu^2)]} \qquad (6.1)$$

here '$C^l$ 'is the velocity of sound , '$E$' is the Young's modulus, '$\rho$' is the density and '$\nu$' is the Poisson ratio of the material.

The velocity of shear wave in a solid medium is given as[107]

$$C^s=\sqrt{(G/\rho)} \qquad (6.2)$$

here '*G*' is the modulus of rigidity of the material. In most cases the relation between these two velocities is[107]

$$C^s = 0.48\, C^l \qquad (6.3)$$

The above equation shows that the elastic properties of the material influence the velocity of ultrasound in that material. In this experiment we could not calculate the value of '*E*' for any of the sample due to the brittle nature of the material. But the very low bending stiffness of the material give an idea that the elastic properties of these materials are in a very low range. Velocity is also related to the frequency and wavelength as[107],

$$C = \lambda * f \qquad (6.4)$$

here '$\lambda$' is the wavelength and' *f*' *is* the frequency of the wave.

Considering the above relations and the results shown in Figure 5.8, it can be observed that the velocity of wave in these materials is quite low. This is also reprehensive of the fragile elastic properties of the materials. When the wave travels in the medium composed of two different materials, its behavior will change at the interface of the two materials[107]. Part of the wave will transmit in the second material and part of wave reflects back to the first medium with a phase change. This depends also on the velocity of sound and the density of both materials, and is termed as 'Specific Acoustic Impedance[107]. In this work the interface of gold NPs and the sorbitol does not seem to transmit the large part of wave. The velocity of sound in bulk gold is 2020m/s and has a resonant frequency of 1.72MHz. If the gold has improved properties at nanoscale or same as bulk gold its resonant frequency should be able to influence the

RUS spectrum of composite. Considering the properties of gold it is expected that the resonant spectra of Au-sorbitol must show visible peaks. After the above discussion, the reasons of absence of gold in RUS spectra can be due to:

- Low concentration of gold NPs, causing no NP-NP interaction
- Shrinkage gap between the NPs and sorbitol, hampering the travel of the wave at the interface influencing the elastic properties, or
- Complete covering of NPs by sorbitol due to weak adhesion or a chemical bonding does not let NPs to vibrate.

This shows that the interfacial properties of metal/matrix in a nanocomposite are important. All the elastic properties are dependent on the interfacial forces. This work shows that for dynamic test based on ultrasounds, concentration of material is the most influencing factor. In case of nanoparticles, a wave of low wavelength (in nanometer range) can detect the particle, otherwise it will cross the particle without traveling through it. The least wavelength that can be obtained using the RUS equipment in our lab is in micrometer (µm) range. When alumina Ø20µm were tested using the RUS, resonance frequency appeared in the spectra, see Fig 5.9. This shows that, in case of matrix material of low sound velocity, very low wavelength waves are required to get useful information about nanocomposite using RUS.

## **6.4.** Remarks

Interfacial forces greatly influence the morphological and mechanical properties of nanocomposite. Shape, size, and concentration were found to affect the morphological and mechanical properties of nanocomposite.

# CHAPTER VII

# PROPERTIES OF GOLD COLLOIDS

This chapter discusses the properties of fluids containing AuNPs as described in Chapter V. The Au colloid with different shapes and sizes of NPs are used in this experiment. The focus of this chapter is to briefly describe the variation in shear and viscous behavior of these colloids with changes in shapes and sizes.

## **7.1.** Non-Newtonian Fluid

The different properties of Au colloid, such as viscosity, shear stress, and shear rate were determined. That was done using an AR G2 (TA Instrument) Rheometer. Results were shown in Chapter V, Figures 5.10-5.13. Results have indicated that the AuNPs fluid was a non-Newtonian fluid that has both thinning and thickening behavior.

In general the velocity of a fluid between the plates is not the same but the fluid flows in parallel planes where each plane has a different velocity relative to the other. This phenomenon was described in Newton's law of friction[108]. Figure 7.1 shows the velocity gradient for the Newtonian fluid held between two plates.

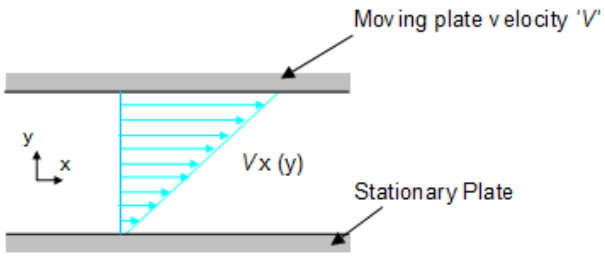


FIG. 7.1. Velocity profile of a Newtonian fluid held between two parallel plates[108]

The resistance to flow offered by these planes relative to another, due to the internal molecular friction that exists between adjacent layers, is termed as viscosity of fluid[108]. The stress required to move these parallel layers or plane, past the other is called shear stress of fluid[108]. If the shear stress of the fluid is in direct relation with velocity gradient in the adjacent planes or layers of fluid, the fluid is called the Newtonian fluid[108], otherwise the fluid is called non Newtonian fluid[108]. Mathematically the relation of shear stress and viscosity of Newtonian fluid is described as, [106]

$$\tau = \mu \frac{\partial v}{\partial y}_{y=0} \tag{7.1}$$

where $\tau$ is the shear stress, $\mu$ is the viscosity of fluid and $\frac{\partial v}{\partial y}$ is the velocity gradient in fluid held between two surfaces separated by a distance "$y$". So in Newtonian fluid shear stress and shear strain have a direct relation and viscosity of fluid is the constant of proportionality.

Non-Newtonian fluid, on the other hand, doesn't show constant viscosity ($\mu$) under different shear rates. Fluid can show shear thickening behavior, increase in viscosity with increase in shear rate, or shear thinning behavior, decrease in viscosity with increase in shear rate. Most of the fluids used in the industry are non-Newtonian. This includes slurries, suspensions, different types of coatings etc. These fluids change their viscosity differently depending on the type of shear and the type of deformation they experience under applied force.

**7.2.** Interfacial Forces in Nanostructured Fluid

In this work gold colloid containing nanospheres and nanorods with different sizes and concentration were tested to measure the viscosity and shear stress at constant shear rate. During testing, different forces can exist between a particle and fluid and between particles as well. These forces are illustrated in Figure 7.2.

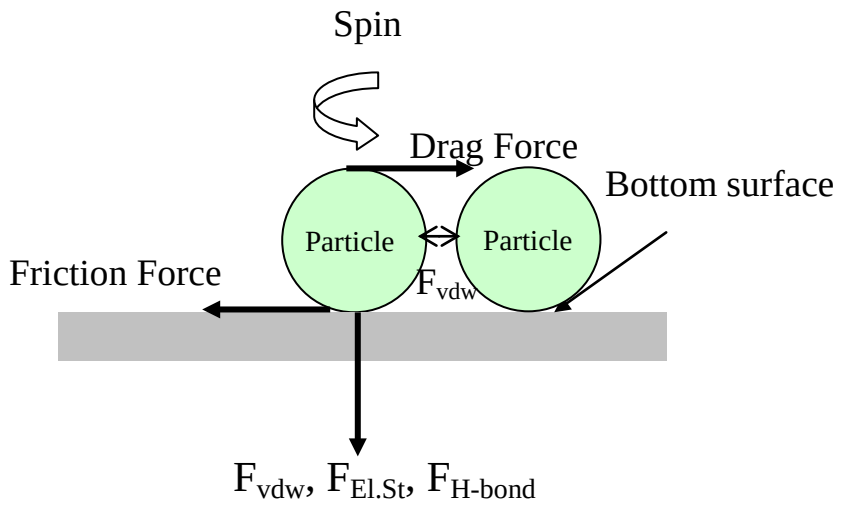


FIG. 7.2. Possible forces during testing of colloid

Due to the rotation of the plate the colloid flows between the plates. This causes a drag force and moment on the liquid resulting in a friction force between the liquid and the surface. Other forces are the interfacial forces between the particles in the liquid and the surface are the van der waal forces and the electrostatic forces. Due to the presence of aqueous solution, hydrogen bonding is also present. Figures 5.10-5.13 show the change in the viscosity and shear stress of different Au colloids. When the shear rate is

small, shear thinning is observed in spherical shaped NPs colloid irrespective of the size of NPs. This behavior of shear thinning for real fluids is usually approximated by power law as[108](equation 7.2),

$$\mu = K(\frac{\partial v}{\partial y})n \qquad (7.2)$$

where $\mu$ is the viscosity, $K$ is the flow index , $(\frac{\partial v}{\partial y})$ is the shear rate, $n$ is the flow behavior index. The value of 'n' ranges from $1 \leq n$ to $1 \geq n$. If the value n=1, it shows that the fluid is Newtonian fluid. In this experiment at low shear rates, the value of 'n' is found to be 0.2333 which is less than 1, while at high shear rates the value of 'n' is higher than 1. Therefore, the fluid of NPs has a non- Newtonian behavior.

## **7.3.** Effects of Au Nanoparticles on Shear Properties of Colloid

### **7.3.1.** Effects of Size of Au Nanospheres on Shear Properties

Figures 5.10. A-B provided the comparison of the shear and viscosity of different sized nanospheres. The volume of colloid was fixed for each specific shape. Despite of size, non-Newtonian behavior was observed for all samples at low and high shear stresses. Decreasing the size increased the no. of particles that affected the shear stress. The specific surface area of diameter 8nm spheres was three times of the diameter 25nm (Figure 7.3).

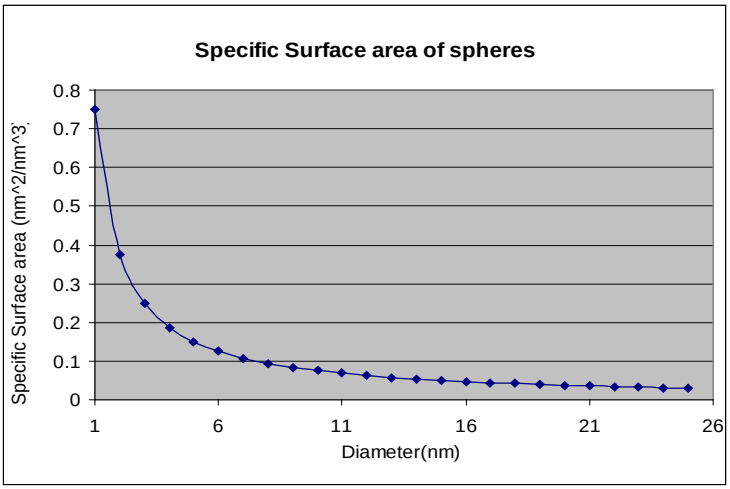


FIG. 7.3. Specific surface area of nanosphere as a function of its diameter

There are clear effects of diameter on Rheological behavior, as shown in Figure 5.10.A-B. At beginning with a low shear rate, all colloid suffered shear thinning. Bigger particles offered more resistance to flow as compared with smaller particles. With changing size, the colloids of the same volume possessed different number of particles. Small particles in a fluid moved easier than the large ones. At low shear rates the particles try to align themselves in the direction of flow. This creates less resistance to flow and the viscosity decreases. This behavior is more pronounced in small size particles as compared to large ones. Smaller particles readily align in the streamline of flow and the viscosity decreases. The less mobility of large particles would offer more resistance to fluid.

The electrostatic forces between the particles and the fluid influenced the smaller particles more than bigger ones. As a result, it helped in keeping the fluid comparatively stabilized at low shear rate. At high shear rates the spinning of particles causes the

particles to move toward the center. The electrostatic forces become less effective as the particle start aggregating, the van der waal forces start influencing the shear behavior. The water film surrounding the particles would not be able to provide sufficient lubrication, so that the adjacent particles will experience friction. This increases the resistance to flow and viscosity and shear stress increases.

### **7.3.2.** Effects of Shape of Au Nanoparticles on Shear Properties

In case of colloids the velocity gradient in different layers of fluid is affected by the size and shape of the particle. If the shape of the particle is changed the surface area will change. In the present research, the rod containing fluid has lower viscosity than that of sphere due to the high surface area. It was discussed that the interactions between NPs and water molecules were stronger than the water-water molecules. This addition of NPs was expected to increase the resistance of shear. Figure 5.13.B, shows the short rods with higher aspect resisted the flow more than the longer rods.

### **7.3.3.** Effects of Concentration of Au Nanoparticles on Shear Properties

Same volume of colloid was tested to check the effect of concentration. Increase in the concentration of particles changes the number of particles and the total surface area of the particles. Difference in surface area causes the difference in the value of viscosity and shear stress at different shear rate. The shear thinning and thickening is determined by the intermolecular forces between molecules in the fluid. As we had discussed, the interfacial interactions between particles and water molecules are stronger than the water

molecules along. Thus in general, the addition of NPs would increase the interactions. But this interaction depends largely on the shapes and sizes of the AuNPs.

The difference in the starting value of viscosity for different sizes of colloid is due to the difference in the specific surface area of the particles. All colloids have the same volume of gold but have particles of different sizes. Difference in the size of particles changes the number of particles and the surface area of the particles. Difference in surface area causes the difference in the starting value of viscosity.

Figure 7.3 shows the specific surface area increase with the decrement in the size of spherical particles. After Ø5nm NPs there is a sharp increase in the specific surface area of the NPs. For the particle size of Ø20nm and above there is almost no significant increase in the specific surface area of the NPs. It may be the reason of unusual viscosity and shear behavior of Ø20nm comare to Ø8nm and Ø75nm gold colloid. It can also be possible that nanospheres of Ø20nm - Ø25nm, define the transition in properties from bulk to nanoscale, as seen in Chapter I.

### **7.3.4.** Effects of Surface Area of AuNanoparticles on Shear Properties

The factors, (size, shape, and concentration), influencing the properties of colloid are all related to the change in surface area of nanoparticles. The discussion above shows that when the surface area was changed by altering either the size, or shape of the particles, the properties of fluid were subseqnetly changed. To see this effect mathematically, the plots of Figure 5.10.A were approximated using the least square method.

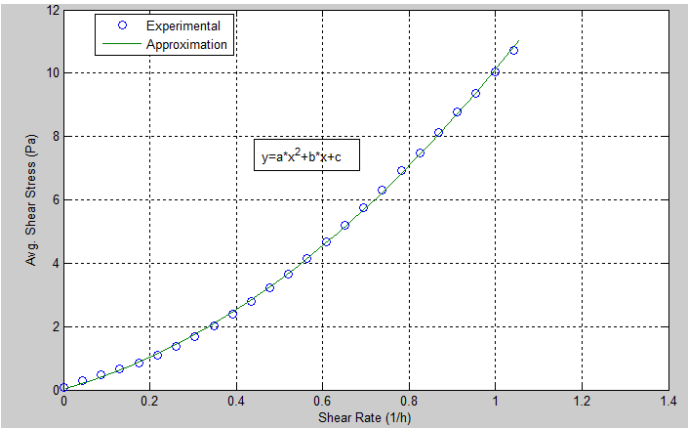


FIG. 7.4.A Curve fitting result of shear stress vs. shear rate plot of Figure 5.10.A, for Ø8nm colloid.

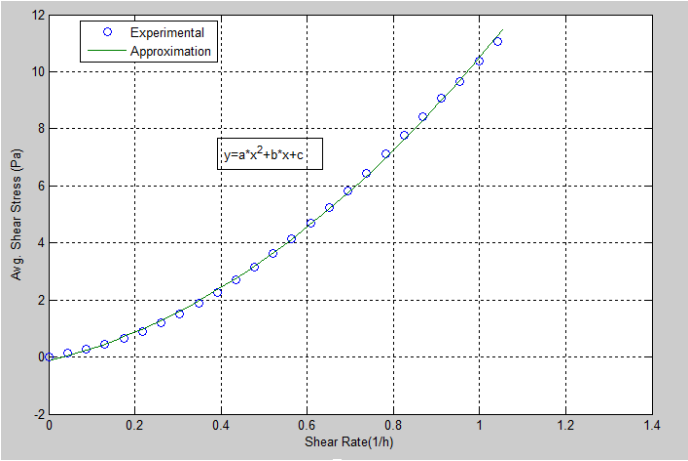


FIG. 7.4.B. Curve fitting result of shear stress vs. shear rate plot of Figure 5.10.A, for Ø75nm colloid.

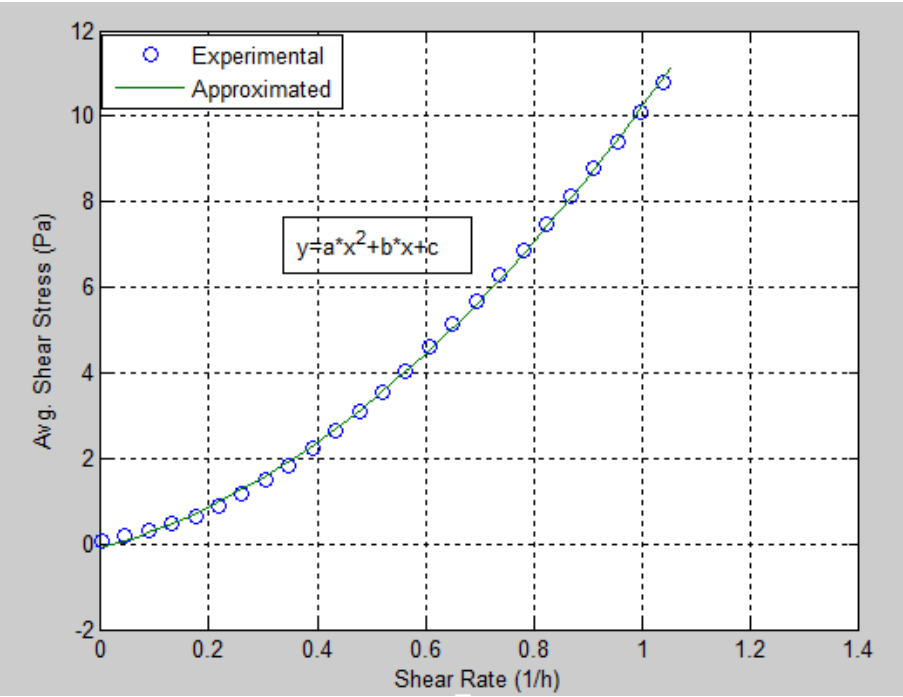


FIG. 7.4.C. Curve fitting result of shear stress vs. shear rate plot of Figure 5.10.A, for Ø25nm colloid.

The following equation (7.3) was obtained and the results are shown in TABLE VI.

$$y=a*x^2+b*x+c \qquad (7.3)$$

here 'y' is the average shear stress(Pa) and 'x' is the shear rate (1/h). The parameters of a, b, and c are listed in TABLE VI, based on results shown in Figures 7.4.A-C. In order to see the relationship between the surface area and those paratmers, the former is listed in the table.

As discussed in Chapter III, due to the fixed volume of gold used in these colloids the expected number of particles in colloids(of different shapes and sizes) were

caluculated as listed in TABLE II. The total surface area based on the those number of particles (TABLE II) is listed in TABLE VI, below.

TABLE VI. The values of coefficients of eq.7.3 for different surface areas of NPs

| S. No. | Surface area of NPs in colloid ($nm^2$) | Coefficients of eq.(7.3) | | |
|---|---|---|---|---|
| | | a | b | c |
| 1 | $4.78x10^{15}$ | 7.3955 | 3.1428 | 0.1559 |
| 2 | $2.39x10^{15}$ | 6.42 | 3.6661 | 0.043 |
| 3 | $1.53x10^{15}$ | 6.0051 | 3.7629 | -0.0328 |
| 4 | $7.65x10^{14}$ | 6.8958 | 3.3949 | -0.0815 |
| 5 | $2.55x10^{14}$ | 7.7068 | 3.5533 | -0.1252 |

The above table shows that the coefficients seem to be related to the surface area of the NPs. The values of the coefficients are increasing with the increase in the surface area of particles. But the values of coefficients in some colloids (TABLE VI, S.No.4&5) are showing an opposite trend. This shows that surface area of the nanoparticles is not the only factor that influence shear behavior. To further explain this simple interpolation was carried out in the experimental data given in Figures 5.10.A-E, to calculate the shear properties of colloids, for same surface area of particles in each colloid. The shear properties of these colloids are summarized in Figure 7.5. Each curve in Figure 7.5 is

obtained using the same surface area value, $2.55x10^{14}$ $nm^2$, of nanoparticles in colloids. Details of calculation of this surface area are given below.

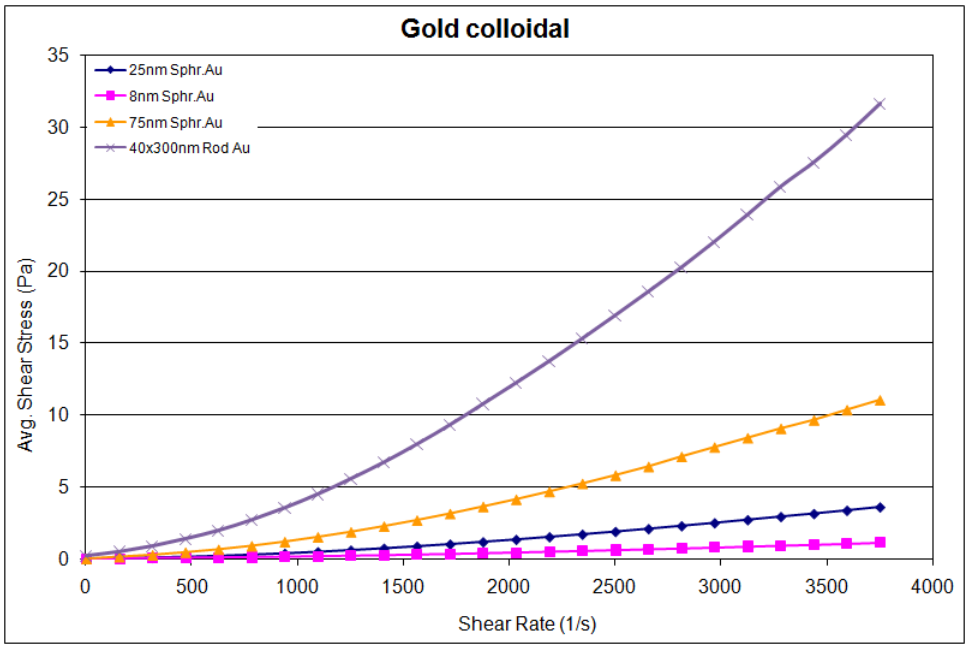


FIG. 7.5. Shear stress vs. shear rate plots of different colloids having same surface area of nanoparticles.

The surface area of each colloid was different due to the size of the particles. The total numbers of particles are known through synthesis of fixed weight of gold salt. The total surface area is then obtained by multiplying the surface area of each particle and the total number particle. Since the Ø75 nm colloid has the least surface area of NPs. The surface area of this colloid is 2.55x10^14 nm2 taken as the reference. Then the shear stress is calculated to be uniform based on this area. The data is then plotted in Figure 7.5. Under our assumption of uniformed surface area, the shear stress and shear rate as

significantly different. This means that the surface area plays an important role. Our experimental data has indeed proven this (Figure 5.11 and 5.12). The larger the surface areas, the higher the particle resistance to fluid shear. This indicates the importance of the interfacial forces between fluid and particles.

## **7.4.** Remarks

Based on the preliminary analysis of effects of size and shapes, the surface area plays an important role in the fluid behavior. The higher the surface area, the higher the shear stress at a certain shear rate. Shear rate influences the interaction of particles with fluid and also interaction among particles. This influences the interfacial forces among particles and between particles and fluid, so that the properties of fluid changes.

# CHAPTER VIII

## CONCLUSIONS AND FUTURE RECOMMENDATIONS

In these thesis effects of shapes, sizes and concentration of Au NPs on the properties of composite and colloid were studied. Morphological investigation was firstly done on AuNPs-sorbitol composite. Effects of concentration were observed in the morphology. The mechanical properties of Au nanocomposite were determined. Both static and dynamic techniques were used to evaluate the shape and size effects on the mechanical properties of the composite. Finally, a dynamic technique was utilized to check the shape and size effects on the shear properties of an Au colloid. There are three major scientific achievements in this research.

For the first time, we used high resolution and spectroscopic techniques to study the nanocomposite. Understanding was obtained in principles of characterization techniques in regards to the size and shape of nanoparticles in order to evaluate the effectiveness of surface characterization techniques.

The interfacial forces play important roles in mechanical properties of materials in their solid and liquid state. In the solid date, the sorbitol molecules around the NPs were weakened due to shrinkage resulting in reduced flexure modulus. In liquid, there was a transition of roles between particle size or surface area and the interfacial forces.

It was found that the interfacial areas between NPs and fluid molecules were responsible for the fluid thinning. Also if the surface area of the NPs is same in all colloid, the size of the particle contributed in the change of viscosity at high and low

shear rates. At high shear rate the interfacial forces between particles contributed in the fluid thickening.

Future Recommendations are as follows:

a. More characterization needs to be done for the AuNPs-sorbitol interaction.
b. Potential applications of sorbitol (for grafting Au NPs) in biosensors and electrodes, is recommended to be considered.
c. The behavior of Ø25nm was interested and needs to be further investigated.

## REFERENCES

[1] H.S. Nalwa, (Ed.)**,** *Encyclopedia of Nanoscience and Nanotechnology* (American Scientific Publishers, Valencia, CA, 2004).

[2] M. Hosokawa, K. Nogi and M. Naito, *Nanoparticle Technology Handbook* (Elsevier, Amsterdam, 2007).

[3] B. Bhushan, *Springer Handbook of Nanotechnology* (Springer, New York, 2007).

[4] W. A. Goddard, *Handbook of Nanoscience, Engineering, & Technology* (CRC Press, Boca Raton, FL, 2003).

[5] A. D. McFarland, J. Chem. Educ. **81**, 544A (2004).

[6] K. Tapan, J.NP.Res. **3**, 257 (2001).

[7] V. F. Puntes and K. M. Krishnan, Science. **291**, 2115 (2001).

[8] U. Kriebig and M. Vollmer, *Optical Properties of Metal Clusters* (Springer, Berlin, 1995).

[9] S. A. Sapp and D. T. Mitchell, Chem. Mater. **11,** 1183 (1999).

[10] L. Sun, P. C. Searson and C. L. Chien, Phys. Rev. B.**61**, R6463 (2000).

[11] M. Yoshida and H. Ogiso, Rev. Sci. Instrum.**76**, 093905 (2005).

[12] W.W. Gerberich and W. M. Mook, J. Mech. Phys. Solid. **51**, 979 (2003).

[13] T. Kizuka and Y. Takatani, Phys. Rev.B.**72**, 035333 (2005).

[14] M. J. Stowell and T. J. Law, Proc. Roy. Soc. London A. **318**, 231 (1970).

[15] G. L. Allen and R. A. Bayless, Thin Solid Films. **144**, 297 (1986).

[16] N. T. Gladkikh and L. K. Gregoriva, Sov. Phys. Solid State. **31**, 728 (1989).

[17] K. Ishikawa and K. Yoshikawa, Phys. Rev. B. **37**, 5852 (1988).

[18] H. Suzuki and T. Ohno, J. Soc. Powder Technol.Jpn. **39** (12), 877 (2002).

[19] R. J. Pressley, *Handbook of Laser with Selected Data on Optical Technology* (The Chemical Rubber Co., Cleveland, 1971).

[20] C. Kittel and P. McEuen, *Introduction to Solid State Physics* (Wiley, Hoboken, NJ, 2005).

[21] K. Kajikawa, Jpn. Opt. **33**, 159 (2004).

[22] T. Mitsui and T. Sekiguchi, *Comparison of Cathodoluminescence & Scanning Near Field Optical Microscopy for Semiconductor Quantum Dots*', 2nd Intl. Workshop, Tokyo (Japan), (www.brl.ntt.co.jp/conference/nss2) (2002).

[23] H. Nishio and Y. Ota, J. Magn, Magn, Mater. **287**, 234 (2005).

[24] K. Hayashi and K. M. Oshugi, Electrochem. Solid State Lett. **5** (7), J9 (2002).

[25] H. Maeda, J. Control. Release. **19**, 315 (1992).

[26] K. Uchino and E. Sadanaga, J. Am. Ceram. Soc. **72** (8), 1555 (1989).

[27] H. Suzuki and T. Ohno, J.Soc.Powder Technol., Jpn. **39**, 877 (2002).

[28] H. Kung and T. Foecke, MRS Bull. **24**, 14 (1999).

[29] R.W. Siegel and G. E. Fougere, Nanostructured. Material. **6**, 205 (1995).

[30] N. Tsuji and R. Ueji, Scr.Mater. **46**, 305 (2002).

[31] C. E. Bottani, G. Benedek, *Nanostructured Carbon for Advanced Applications* (Kulwer Academic, Boston, 2001).

[32] N. Moszner and U. Salz, Prog. Polym. Sci. **226**, 535 (2001).

[33] M. Alexandre and P. Dubois, Mater. Sci. Eng. **28**, 1 (2000).

[34] P. R. Goglia and J. Berkowitz, Diamond Relat. Mater. **10**, 271 (2001).

[35] J. He and J. M. Schoenung, Surf. Coat. Technol. **157**, 72 (2002).

[36] M. L. Roukes, Phys.World. **14**, 25 (2001).

[37] M. L. Roukes, *Solid State Sensor and Actuator Workshop*, Hilton Head, SC, 367 (2000).

[38] M. Nastasi, D. M. Parkin, and H. Gleiter, *Mechanical Properties and Deformation Behavior of Materials Having Ultrafine Microstructures* (Kluwer, Dordrecht, 1993).

[39] N. E. Dowling, *Mechanical Behavior of Materials (*Pearson Prentice Hall, London, 2007).

[40] K. K. Chawla and M. A. Meyers, *Mechanical Behavior of Materials*, (Cambridge University Press, New York, 2009).

[41] D. Hull and D. J. Bacon, *Introduction to Dislocation, 3rd ed*. (Pergamon Press, Oxford, 1984).

[42] G. E. Dieter, *Mechanical Metallurgy* (McGraw Hill, New York, 1986).

[43] M. Jose, J. Ascencio and H. B. Liu, J. Vac. Sci. Technol. B. **19** (4), 1091 (2001).

[44] H. H. Read, *Rutley's Elements of Minerology*, 26th Ed. (Thomas Murby & Co., London, 1970)

[45] C. L. Cleaveland and U. L. Landman, Phys.Rev.Leters. **79**, 1873 (1997).

[46] A. L. Mackay, Acta. Cryst. **15**, 916 (1962).

[47] C. L. Cleaveland and U. L. Landman, J. Chem. Phys. **94**, 7379 (1991).

[48] A. N. Pail, D. Y. Paithankar and N. Otsuka. Phys. D: At., Mol. Clusters. **26**, 135 (1993).

[49] C. Gutierrez-Wing and P. Santiago, Appl, Phys. A: Mater. Science Process. **70**, 1 (2000).

[50] G. W. Niemen and R.W. Siegel, J. Mater. Res. **6**, 1012 (1991).

[51] X. Zhu, R. Birringer and U. Gonser, Phys. Rev. B. **35**, 9085 (1987).

[52] U. Herr and R. Birringer, Appl. Phys. Lett. **50**, 472 (1987).

[53] T. Haubold and R. Birringer, J. Less Common Metals. **145**, 557 (1988).

[54] T. Haubold and R. Birringer, Phys. Lett. A. **135**, 461 (1989).

[55] H.S. Kim and M. B. Bush, Nanostruct. Mater. **11**, 361 (1999).

[56] S.Veprek and A. S. Argon, J. Vac. Sci. Technol. B. **20**, 650 (2002).

[57] G. Hartland, SPIE. 10.1117/2.1200604.0168 (2006).

[58] H. Tanimoto and H. Sakai, Nanostruct. Mater. **12**, 751 (1999).

[59] M. Weller and J. Diehl, Philos. Mag. A. **63**, 527 (1991).

[60] D. Chen, Mater. Sci. Engr. A.**190**, 193 (1995).

[61] G. J. Thomas and R.W. Siegel, Scripta Metall Mater.**24**, 201 (1990).

[62] G.W. Nieman, *Ph.D Dissertation*, Northwestern University Evanston, IL (1991).

[63] P. Gao and H. Gleiter, Acta Metall. **35**, 1571 (1987).

[64] W. Milligan and S. A. Hackney, Nanostructured Mater. **2**, 267 (1993).

[65] D. G. Morris and M. A. Morris, Acta Metall. Mater. **39**, 1763 (1991).

[66] M. Jain and T. Christman , Acta Metall Mater. **41**, 1431 (1993).

[67] B. Gilbert, Science, **305**, 651 (2004).

[68] D. Wolf and J. F. Lutsko, Phys. Rev.Lett. **60**, 1170 (1988).

[69] R. Cammarata and K. Sieradzki, Phys. Rev. Lett. **62**, 2005 (1989).

[70] C. Johnson and E. Snoeck, Nature Matls. **7** (2), 120 (2008).

[71] R.W. Siegel and S. Ramasamy, J. Mater. Res. **3**, 1367 (1988).

[72] H. Schaefer and R. Wurschum, Mater. Sci. Forum. **15**-18, 955 (1987).

[73] H. Schaefer and R. Wurschum, Phys. Rev. B. **38**, 9545 (1988).

[74] H. Hahn and J. Logas, J. Mater. Res. **5**, 609 (1990).

[75] W. Wagner and R. Averback, J. Mater. Res. **6**, 2193 (1991).

[76] P. G. Sanders and J. Weertman, Scripta Metall Mater. **29**, 91 (1993).

[77] A. Guinier and G. Fournet, *Small Angle Scattering of X-rays* (John Wiley & Sons, New York, 1955).

[78] D. Lozanne, Science, **2561**, 10.1126 (2001).

[79] *AR-G2 Rheometer, Product Manual* (TA Instruments, New Castle (DE) , 2008).

[80] World Gold Council, (www.gold.org) (September 15, 2008).

[81] C. N. Reeves, *Egypt's False Prophet: Akhenaten* (Thames & Hudson, London, 2001).

[82] M. B. Cortie and E. van der Lingen, Materials Forum. **26**, 1 (2002).

[83] K. Dick, T. Dhanasekaran, Z. Xhang, and D. Meisel: J. Am. Chem. Soc. **124** (10), 2312 (2002).

[84] H.B. Liu, J. A. Ascencio, M. Perez-Alvarez, and M. J. Yacaman, Surface Science. **491**, 88 (2001).

[85] H. Richardson and S. Govoro, *Report*, Ohio University Nanobiotechnology Initiative, (www.phy.ohiou.edu) (April 03, 2006).

[86] S. Maier, *Plasmonics: Fundamentals and Application (*Springer, New York, 2007).

[87] S. I. Taniguchi and M. Minamoto, J. Mater. Chem. **16**, 3459 (2006).

[88] W. Eberhardt, Surface Science. **242,** 500 (2002).

[89] Y. Y. Lim and M. M. Chaudhri, Philos. Mag. A. **82** (10), 2071 (2002).

[90] D. M. Schaefer and A. Patil, Phys. Rev. B. **51**, 5322 (1995).

[91]M. El-Sayed, *Report*, Laser Dyanamics Laboratory, Georgia Tech University, (ldl.gatech.edu) (November 30, 2008)

[92] J. Sun, Langmuir, **25** (1), 451 (2009).

[93] J. S. Lee, *Lectures,* Kookmin University, Seoul. (Spring 2008)

[94] J. S. Turkevich and P. L. Hillier, J. Discuss. Faraday Soc. **11**, 55 (1951).

[95] P. C. Champe, R. A. Harvey and D. R. Ferrier, *Biochemistry* (Lippincott/Williams & Wilkins, Philadelphia, 2005).

[96] D. Briggs and M. P. Seah, *Practical Surface Analysis* (Wiley, New York, 1992).

[97] L.V. Azároff, *X-Ray Diffraction* (McGraw-Hill, New York, 1974).

[98] Nanoscience Instruments, Inc, (www.nanoscience.com) (January 16, 2009).

[99] *Resonant Ultrasound Spectroscope, Product Manual*, (Quasar Intl, Albuquerque, NM, 2008).

[100] A. Migliori and J. L. Sarrao, *Resonant Ultrasound Spectroscopy* (J. Wiley, New York, 1997).

[101] B. J. Zadler, L. Rousseau, H. L.Jérôme, J. A. Scales and M. L. Smith, Geophysical Journal International, **156,** 1 (2004).

[102] M. Radovic, Material Science & Engineering A. **368** (1-2), 56 (2004).

[103] Y. Liu, J. Am. Ceram. Soc. **80** (1), 142 (1997).

[104] M. P. Casaletto, Interface Anal. **38**, 215 (2006).

[105] K. M. Doll, Journal of Polymer Science: Part A: Polymer Chemistry.**44**, 4259 (2006).

[106] C. Peng, Aerosol Science and Technology. **35**, 753 (2001).

[107] B. Carlin, *Ultrasonics* (McGraw Hill, New York, 1960).

[108] B. R. Munson, *Fundamentals of Fluid Mechanics*, (John Wiley & Sons, New York, 1940).

# VITA

.

Tahira Zarrin received her Bachelor of Engineering degree in mechanical engineering from NED University of Engineering and Technology at Karachi (Pakistan) in 1999. She entered Texas A&M University in January 2007 to pursue Master of Science degree in mechanical engineering. Her research interest includes the characterization of nanoparticles and the determination of methodology for the precise evaluation of mechanical properties of nanoparticles and or nanocomposite.

Ms. Tahira can be contacted at the Mechanical Engineering Department at Texas A&M University, College Station, TX, 77843-2123. Her email address is tzarrin@gmail.com.